HHS Public Access

Author manuscript

Nat Nanotechnol. Author manuscript; available in PMC 2022 April 25.

Published in final edited form as:

Nat Nanotechnol. 2021 December ; 16(12): 1424–1434. doi:10.1038/s41565-021-00982-5.

Nano-Optogenetic Engineering of CAR T-cells for Precision Immunotherapy with Enhanced Safety

Nhung Thi Nguyen[1,#], **Kai Huang**[2,#], **Hongxiang Zeng**[3], **Ji Jing**[1], **Rui Wang**[1], **Shaohai Fang**[3], **Joyce Chen**[4], **Xin Liu**[1], **Zixian Huang**[1], **M. James You**[5], **Anjana Rao**[4], **Yun Huang**[3,6,*], **Gang Han**[2,*], **Yubin Zhou**[1,6,*]

[1]Center for Translational Cancer Research, Institute of Biosciences and Technology, Texas A&M University, Houston, TX 77030, USA

[2]Department of Biochemistry and Molecular Pharmacology, University of Massachusetts Medical School, Worcester, MA 01605, USA

[3]Center for Epigenetics and Disease Prevention, Institute of Biosciences and Technology, Texas A&M University, Houston, TX 77030, USA.

[4]Division of Signaling and Gene Expression, La Jolla Institute for Immunology, La Jolla, CA, USA

[5]Department of Hematopathology, The University of Texas MD Anderson Cancer Center, Houston, Texas, 77030, USA

[6]Department of Translational Medical Science, College of Medicine, Texas A&M University, Houston, Texas 77030, USA.

Abstract

FDA-approved chimeric antigen receptor (CAR) T cell-based immunotherapy has shown curative potential in patients with hematological malignancies. However, owing to the lack of control over the location and duration of anti-tumor immune response, CAR T-cell therapy still faces significant safety challenges arising from cytokine release syndrome and on-target off-tumor toxicity. Herein, we present the design of light-switchable CAR T-cells (designated “LiCAR-T”) that allow real-time photo-tunable activation of therapeutic T cells to precisely induce tumor cell killing. When coupled with imaging-guided, surgically removable upconversion nanoplates

[*]MANUSCRIPT CORRESPONDENCE: Institute of Biosciences and Technology, Texas A&M University, Houston, TX 77030, USA OR, Department of Biochemistry and Molecular Pharmacology, University of Massachusetts Medical School, Worcester, MA 01605, USA, Y Zhou (lead contact; yubinzhou@tamu.edu), or G Han (Gang.Han@umassmed.edu), or Y Huang (yun.huang@tamu.edu).
[#]These authors contributed equally to the work.

AUTHOR CONTRIBUTIONS

Y.Z., G.H. and Y.H. conceived the study. Y.Z., G.H. and N.T.N. designed the experiments; N.T.N., H.Z., J.J., R.W., S.F., Z.H., X.L., and K. H. performed the experiments and data analysis; K.H. synthesized, characterized nanoparticles, and interpreted EDS data; G.H.., J.C., Y.H., M.J.Y, and A.R. provided intellectual inputs and scientific feedbacks, as well as suggestions for animal models; Y.Z., Y.H., N.T.N., K.H. and G.H., wrote the manuscript. All authors provided feedbacks and helped shape the research, data analysis and the manuscript.

Competing Interests

Y.Z. and G.H. have submitted a patent application to the United States Patent and Trademark Office pertaining to the design and biomedical applications aspect(s) of this work (application number 62/942,770). The remaining authors declare no competing interests.

(UCNPs) that have enhanced near infrared (NIR)-to-blue upconversion luminescence as miniature deep tissue photon-transducers, LiCAR T-cells enable both spatial and temporal control over T cell-mediated anti-tumor therapeutic activity in vivo with greatly mitigated side effects. Our nano-optogenetic immunomodulation platform not only provides a unique approach to interrogate CAR-mediated anti-tumor immunity, but also sets the stage for developing precision medicine to deliver personalized anti-cancer therapy.

Chimeric antigen receptor (CAR) T-cell immunotherapy has demonstrated great potential for tumor eradication[1]. CARs are synthetic receptors engineered into the plasma membrane (PM) of effector T cells, where they engage specific tumor antigens in a major histocompatibility complex-independent manner[2]. Antigen recognition allows engineered T cells to be activated and to subsequently perform their tumor killing function. Despite of its success in cancer treatment[1,3,4], CAR T-cell therapy is still fraught with safety challenges due to the lack of precise control over the dose, location, and timing of T cell activity[5], as exemplified by the cytokine release syndrome (CRS) and “on-target, off-tumor” cytotoxicity[5] (e.g., B cell aplasia[6]). Hence, intelligent CAR-T cell-based therapies with precise spatiotemporal control over therapeutic activities are urgently needed.

Herein, we describe the engineering of light-switchable CAR T-cells (LiCAR-T) that can precisely mount anti-tumor immune responses in the dual presence of tumor antigen and light. Because anti-CD19 CAR T-cells have been approved by the FDA to treat hematological neoplasms (Yescarta[7] and Kymriah[4]), we focused our study on the targeting of the CD19 antigen to validate our technology. To demonstrate the feasibility of wireless optogenetic immunotherapy *in vivo*, we further combined LiCAR-T with surgically removable upconversion nanoplates (UCNPs) that have enhanced near infrared (NIR)-to-blue upconversion luminescence. The UCNPs act as miniature light transducers to enable inducible activation of LiCAR T-cells in living animals upon stimulation with deep tissue-penetrable NIR light. This NIR light-tunable nano-optogenetic platform enables spatiotemporal control of CAR T-cell mediated cytotoxicity against both hematological malignancies and solid tumors with tailored doses and duration, thereby greatly mitigating side effects associated with the current immunotherapy.

Design of LiCAR to remotely photo-tune T cell activation

LiCARs were engineered by intracellularly splitting the functional domains of CAR and installing photo-responsive modules into each half of a split CAR (Fig. 1a-b and Extended Data Fig. 1a). In our envisioned design, T cell activation only occurs after the functional assembly of the two components of the split CAR in the presence of blue light, thus conferring spatiotemporal control over the anti-tumor immune response (Fig. 1a). To test this idea, we designed a series of candidate receptors for light-dependent assembly of functional CARs (Fig. 1a-b and Extended Data Fig. 1a). Two optical dimerizers with different kinetic features were utilized. The first pair consisted of the photolyase homology domain of *Arabidopsis* cryptochrome 2 (CRY2) and the N-terminal region of its photo-sensitive binding partner CIB1 (the CRY2/CIBN pair)[8]. The second system, iLID, contains a bacterial peptide ssrA that is fused to the C-terminus of *Avena* light-oxygen-voltage

domain 2 (LOV2), and exhibits light-dependent interaction with its binding partner sspB (the LOV2-ssrA/sspB pair)[9].

Based on these elementary building blocks, we generated a series of hybrid constructs by fusing optical dimerizers with either the extracellular antigen-binding modules or the intracellular signal transduction modules derived from a conventional CAR (Extended Data Fig. 1a). After optimization to improve PM trafficking and reduce the nuclear accumulation of engineered components (Fig. 1b-e, Extended Data Fig. 1b-f, and Supplementary Note 1), we identified the best performing combinations that displayed light-dependent heteromerization in a reversible manner (Fig. 1c-h, and Supplementary Videos 1-2). The varying range of deactivation half-lives of LOV2- and CRY2-based LiCARs makes it possible to temporally control the duration of the elicited anti-tumor immune response.

We next sought to screen combinations that would permit the light-induced functional assembly of LiCARs in T cells by using NFAT-dependent luciferase (NFAT-Luc) expression[10] or IL-2 production to report T cell activation. NFAT-Luc Jurkat T cells expressing engineered receptors (Supplementary Fig. 1) were co-cultured with human CD19 (hCD19)-negative K562 leukemia cells or hCD19-positive Raji lymphoma cells (Supplementary Fig. 2). In the dual presence of cognate tumor antigen ($hCD19^+$) and blue light, we detected a pronounced increase of NFAT-driven reporter bioluminescence, indicating the antigen/light-dependent activation of engineered T cells (Fig. 1i). We employed three additional strategies to continue optimizing LiCARs (Supplementary Note 1), including (i) targeting both components to the PM by adding the transmembrane domain of CD8 and/or the homodimeric DAP10 ectodomain[11-13]; (ii) reordering the positions of intracellular CAR components (Fig. 1b and Extended Data Fig. 1a); and (iii) using weaker versions of iLID to reduce dark activity (Figs. 1i and 2a-b). We ultimately identified ideal combinations for both CRY2- and LOV2-based LiCARs, which led to 39% (A+B3) and 93% (C+D4; Fig. 1i) of the maximal response in the NFAT-Luc assay, respectively. Furthermore, weaker versions of iLID (C+D4.1 with sspB mutant R713Q[9] or C+D4.3 with A58V[14]) were employed to reduce the dark activity (Fig. 1b-i, and Supplementary Video 2). As a stringent control, defective LiCAR T-cells (C+D5) lacking CD3ζ-ITAM did not show discernible antigen/light-dependent changes (Fig. 1i). In both the NFAT-Luc reporter assay and the IL-2 ELISA assay (Fig. 2a-c), LiCAR T-cells exhibited light-dependent activation, suggesting the feasibility of using light to fine-tune the degree of T cell activation.

Because the LOV2-based LiCAR seemed superior to the CRY2-based version (Fig. 2b-c), we focused on the C+D4 and C+D4.1 combinations for further characterization. We monitored the cell surface expression of CD69 as an early event indicative of T cell activity (Fig. 2d). While conventional CAR T-cells only required the hCD19 antigen to activate T cells and boost CD69 expression, LiCAR T-cells showed a light-dependent increase in CD69 expression in the presence of $hCD19^+$ Daudi (Fig. 2d-e) or Raji lymphoma cells (Extended Data Fig. 2). As a control, $CD19^-$ K562 cells did not induce any significant change in CD69 expression. Taken together, these results validated the successful construction of LiCAR to achieve dual input-gated control of T cell activation in a photo-tunable manner.

LiCAR T-cells enable nano-optogenetic tumor killing

A hallmark of CAR T-cells is their ability to induce apoptosis in targeted tumor cells. Controlled activation of CAR T-cells to trigger inducible cytotoxicity against tumors is one of the most desirable features of smart immunotherapy. Hence, we generated LiCAR-expressing human $CD8^+$ T-cells to test their tumor killing ability, by using SYTOX blue staining as readout (Fig. 2f-h, and Supplementary Note 1). Both components of LiCAR were co-expressed in $CD8^+$ T-cells derived from peripheral blood mononuclear cells (PBMC) (Extended Data Fig. 3a-c). Engineered human $CD8^+$ T-cells expressing WT CAR or defective LiCAR were used as positive and negative controls, respectively (Fig. 2f-g, Extended Data Fig. 3d and Supplementary Videos 3-4). We observed a light-dependent boost of tumor cell killing in the LiCAR group with the efficiency comparable to conventional CAR T-cells (Fig. 2g-h). Upon photo-stimulation, positive SYTOX blue staining was noted in Daudi cells engaged by LiCAR T-cells (Fig. 2h and Supplementary Videos 5), but not in the dark group (Supplementary Videos 6). Noncognate tumor cells ($hCD19^-$ K562 cells) survived throughout the assay, regardless of the presence of light. Collectively, LiCAR T-cells were able to mount anti-tumor cytotoxicity toward cognate target cells in the dual presence of tumor antigen and light.

Next, we performed similar *ex vivo* co-culture experiments to examine whether engineered $CD8^+$ T-cells derived from mice would likewise trigger cytotoxicity against cancer cells upon blue light stimulation. To test this, we resorted to a mouse B16-OVA melanoma cell line stably expressing human CD19 (B16-OVA-hCD19)[15] and used the B16-OVA melanoma cells as the CD19-negative control (Supplementary Fig. 3a). WT CAR, LiCAR, and defective CAR constructs were individually transduced into mouse $CD8^+$ T-cells (Supplementary Fig. 3b-c). LiCAR-expressing $CD8^+$ T-cells showed photo-inducible production of IFN-γ[16] (Fig. 3a) and cytotoxicity against co-cultured B16-OVA-hCD19 melanoma cells (Fig. 3b and Supplementary Fig. 3d). By contrast, WT CAR T-cells induced tumor killing in a light-independent manner, whereas defective LiCAR T-cells showed negligible light-induced effects (Fig. 3b and Supplementary Fig. 3d). Collectively, we have demonstrated the successful engineering of photo-switchable CAR T-cells from both human and mice to kill cancer cells derived from hematological malignancies (*e.g.,* lymphoma) and solid tumors (*e.g.*, melanoma).

To further validate inducible and selective tumor killing mediated by LiCAR T-cells *in vivo*, we generated a syngeneic melanoma mouse model by inoculating rodent B16-OVA-hCD19 or B16-OVA melanoma cells into the flanks of C57BL/6J mice[15] (Supplementary Fig. 4). These two cancer cell lines showed comparable growth rates both *in vitro* (Supplementary Fig. 4a) and *in vivo* (Supplementary Fig. 4b), thus ruling out the possibility that hCD19 *per se* might induce the differential growth of tumor cells. We then set out to combine LiCAR T-cells with NIR light-activatable upconversion nanoparticles (UCNPs) to circumvent the limited tissue-penetration issue associated with blue light-activatable optogenetic tools[17]. We used UCNPs as injectable nanoscale light transducers to enable wireless optogenetics[18], thereby obviating invasive procedures, such as implanting micro-LEDs or inserting fiber optics in tissue for light delivery. We have previously employed

this strategy to remotely control Ca^{2+} signaling and the immune system during dendritic cell-based immunotherapy[10,19].

To enhance upconversion luminescence intensity, we designed hexagonal-shape upconversion nanoplates with a core-shell composition of β-$NaYbF_4$:0.5%Tm@$NaYF_4$, in which Yb^{3+} serves as the sensitizer to accept excitation light while Tm^{3+} acts as the emitter (Fig. 3c). Compared to the ~30 nm β-$NaYF_4$:30%Yb,0.5%Tm@$NaYF_4$ core-shell UCNPs used previously[10], this new design incorporated an elevated Yb^{3+} concentration (99.5%) and enlarged nanoparticle size (~200 nm in diameter and ~85 nm in height)[25] to enhance upconversion luminescence (Fig. 3d-e, Extended Data Fig. 4a-b and Supplementary Note 2). When excited at 980 nm, these UCNPs exhibited intense blue emission, with a 4.5-fold intensity enhancement compared to the conventional UCNPs (Fig. 3e and Extended Data Fig. 4c). To make them more biocompatible, a silica shell was coated on the UCNP surface (Fig. 3d and Extended Data Fig. 4b) without compromising their upconversion luminescence (Extended Data Fig. 4d and Supplementary Note 2). When the silica-coated UCNPs were subcutaneously injected into mice, we detected bright blue emission from the injection site under NIR light illumination (Extended Data Fig. 4e). We further systematically examined the biocompatibility of these UCNPs (Supplementary Note 2). Through a series of *in vitro* and *in vivo* biosafety studies, we confirmed that these silica-coated UCNPs did not significantly affect the cell viability (Supplementary Fig. 5a) or the blood test results (Supplementary Table 1), nor induce noticeable organ damages, inflammatory lesions (Supplementary Fig. 5b-c) or macrophage dysfunctions (Supplementary Fig. 5d-e). These results firmly establish the excellent biocompatibility of our silica-coated UCNPs *in vivo*.

To evaluate the ability of LiCAR T-cells to eliminate antigen-specific melanoma masses, we conducted *in vivo* experiments with intradermal melanoma models, in which tumor cells-bearing non-cognate antigen (B16-OVA) and cognate antigen (B16-OVA-hCD19) were implanted into each flank of the same C57BL/6J mice (Fig. 3f-h, and Supplementary Note 2). As the positive control, WT CAR T-cells exhibited tumor antigen-specificity by killing tumors that were made of B16-OVA-hCD19 cells, but not hCD19-negative B16-OVA cells (Extended Data Fig. 5a). As the negative control, the NIR light-treated groups injected with UCNPs alone did not seem to affect the overall tumor growth (Extended Data Fig. 5b-c). These results ruled out the possible complications from UCNPs and NIR light *per se*. For the LiCAR T-cell treated group, NIR light stimulation suppressed B16-OVA-hCD19 tumor growth in the left flank, while CD19-negative B16-OVA tumors on the right flank remained largely unaffected (Fig. 3g and Extended Data Fig. 6a). It is noteworthy that the injected UCNPs appeared to be confined at the injection site or within the tumor mass and thus could be surgically removed after the treatment via upconversion emission imaging guidance (Extended Data Fig. 7). These UCNPs remained structurally intact and did not seem to spread to major organs for at least four weeks, which was confirmed by energy-dispersive X-ray spectroscopy (EDS) coupled SEM analysis (Extended Data Fig. 7, Supplementary Figs. 6-7, and Supplementary Table 2). Taken together, these findings establish that UCNPs tend to be accumulated in the tumor after injection and can be removed by imaging guided surgery without leakage to the surrounding tissue or other organs.

We subsequently analyzed the population of surviving and/or locally expanded LiCAR T-cells within tumor masses 9 days after injection by flow cytometry (Supplementary Fig. 8). As anticipated, a significant portion of dual-colored LiCAR T-cells was detected within the $CD19^+$ tumors, but not in those formed by CD19-negative B16-OVA cells (Supplementary Fig. 8a-b). In addition, we did not observe a significant presence of LiCAR T-cells in the peripheral lymphoid organs or in the peripheral blood at the endpoint (Supplementary Fig. 8c). Taken together, we have established a robust nano-optogenetic platform to temporally control LiCAR T-cells to achieve tumor-specific immune responses *in vivo*.

To demonstrate the spatiotemporal control of LiCAR T-cells with respect to tumors killing *in vivo*, we next implanted B16-OVA-hCD19 cells into each flank of C57BL/6J mice. After tumor formation at day 9, both tumor sites were injected with a mixture of $CD8^+$ LiCAR T-cells and UCNPs, and followed by exposure to pulsed NIR light on the left side or shielded from light with aluminum foil on the right side (Fig. 3h and Extended Data Fig. 6b). We found that tumor regression or clearance was only observed in the NIR light-treated side, not in the site shielded from light (Fig. 3h and Extended Data Fig. 6b). Within the tumor masses, we detected a higher amount of LiCAR T-cells, at day 9 following NIR light stimulation (Supplementary Fig. 8d). In parallel, we performed similar experiments under blue light illumination. We did not detect a statistically significant difference between the dark and lit groups (Extended Data Fig. 8). This finding is consistent with the tacit notion that blue light can penetrate no more than 1 mm in living tissues[20], thereby failing to effectively activate LiCAR T-cells within the tumor sites. Clearly, our data established the feasibility of nano-optogenetic control over engineered T cell activation and selective tumor killing only at the desired tumor sites.

Systematic delivery of LiCAR T-cells for lymphoma killing

In order to better mimic the clinical scenario, we performed systemic administration of LiCAR T-cells via tail vein injection (*i.v.*) and evaluated their ability of selective elimination of lymphoma with NIR light treatment. We tested two parallel methods of UCNP administration: (i) via intratumoral (*i.t.*; Fig. 4a-b) injection of UCNPs, as we illustrated above; and (ii) the intravenous co-delivery of surface-biotinylated LiCAR T-cells and streptavidin-functionalized UCNPs, which is similar to what we did in our previous work[10] (Fig. 4c-f; and Extended Data Fig. 9). In both approaches, the lymphoma was established by subcutaneous implantation of the mixture of 1.5×10^5 Raji cell and Matrigel (1:1) into both flanks of SCID-Beige mice, with one flank exposed to NIR light and the other shielded from photo-stimulation. For the first method, we found that the tumor suppression only occurred on the NIR light-treated side (Fig. 4b). However, the tumor-suppressive effect of LiCAR T-cells was not as prominent as those observed in the intratumoral injection model (Fig. 3g-h). Two reasons might account for the observed difference in tumor-killing efficacy: (i) systemic delivery of CAR T-cells is known to be less efficient than direct intratumoral administration due to inefficient trafficking of CAR T-cells into the hostile tumor microenvironment; (ii) the separated routes of delivering LiCAR T-cells (*i.v.)* and UCNPs (*i.t.*) reduce the optical coupling efficiency.

To improve the coupling efficiency of our nano-optogenetic approach, we conjugated streptavidin (Stv)-functionalized UCNPs to LiCAR T-cells[10, 27] (Extended Data Fig. 9 and Supplementary Note 3). We then administered the Stv-UCNP-LiCAR T-cells via tail vein injection in tumor-bearing mice with two weekly doses (Fig. 4c). The Stv-UCNP-LiCAR T-cells were found to be efficiently accumulated in the tumor, as independently confirmed by eye-visible blue emission under NIR excitation, the element analysis and immunostaining of mouse tissue (Supplementary Fig. 9, Supplementary Table 3, and Supplementary Note 3). With the second approach, we observed more efficient tumor killing in the NIR-treated LiCAR T-cell group (Fig. 4d). As stringent controls, the tumors shielded from NIR light, or those in the control group only receiving LiCAR T-cells (without UNCPs), grew at their full capacity (Fig. 4d-f). Collectively, we have established the feasibility of using Stv-UCNP-LiCAR T-cells for inducible lymphoma killing via systematic injection.

LiCAR T-cells exhibit substantially attenuated side-effects

We next asked whether the LiCAR-T system could mitigate the side-effects associated with conventional CAR T-cells, as most prominently known as “on-target, off-tumor” cytotoxicity and CRS. To evaluate the “on-target, off-tumor” side effects in a syngeneic mouse model of tumor, we designed a new set of mouse-specific LiCARs (mLiCARs; Fig. 5a), in which the hCD19-recognizing scFv was replaced by a mouse CD19 (mCD19)-specific 1D3 ScFv[21]. mLiCAR was found to only recognize the mCD19 antigen and caused activation of NFAT-dependent luciferase expression (Fig. 5b, Supplementary Fig. 10a and Supplementary Note 4). Similar to the human LiCAR system, both WT mCAR and mLiCAR T-cells exhibited tumor antigen-specificity by suppressing the growth of tumors composed of B16-OVA-mCD19 cells, but not the B16-OVA cells (Fig. 5c-d, and Supplementary Note 4), thus validating the on-target effects of mLiCAR T-cells.

B cell aplasia is one of the most frequent life-threatening side effects associated with CD19 CAR T-cell therapy due to the expression of CD19 on both B cell malignant clones and non-pathogenic B cells. In order to evaluate the degree of B cell aplasia, we compared the number of B cells in the peripheral blood obtained from the WT mCAR or mLiCAR-treated groups (as shown in Fig. 5c-d) at the day prior to T cell implantation (day 0) and 3 days thereafter (Fig. 5e). We found that mWT CAR T-cell treatment triggered B cell aplasia after 3 days by reducing both the B cell number (Fig. 5e) and the B cell percentage in the peripheral blood (Supplementary Fig. 10b), while this phenomenon was not observed in the mLiCAR group. The similar scenario was seen in another model via intraperitoneal (*i.p.*) injection of tumor cells (Extended Data Fig. 10). These findings suggest that the UCNP/LiCAR system attenuates the undesired “on-target, off-tumor” toxicity. Additionally, we found that mLiCAR T-cells did not seem to attack major organs during our experimental window (Fig. 5f).

Another prevalent adverse effect following CAR T-cell treatment is the initiation of a cytokine storm associated with uncontrolled immune responses, known as CRS[22]. A dramatic elevation of IL-6 is one of the critical hallmarks of CRS, along with elevated granulocyte macrophage colony-stimulating factor (GMCSF), IFN-γ and IL-10[23,24]. To evaluate the extent of CRS in our system, we adapted a well-established xenograft

model of CAR T-cell-induced CRS in SCID-Beige mice recently developed by Giavridis et al[25], which has been shown to recapitulate major CRS hallmarks seen in the clinic (Supplementary Note 4). After 3 days, the mice treated with WT CAR T-cells experienced significant weight loss (Fig. 6a-b). Furthermore, the level of mIL6 was higher in the tumor-bearing mice injected with WT CAR T-cells compared to those injected with LiCAR T/UCNPs under pulsed NIR light (Fig. 6c), suggesting that the LiCAR system indeed mitigated the cytokine release syndrome.

CONCLUSIONS

In the current study, we described the combination of UCNPs with enhanced upconverting optical performance with LiCAR T-cells to enable wireless control of tumor eradication in diverse mouse models via NIR light, which has been demonstrated to have much deeper tissue penetration. Prior to our study, light-induced expression of the CAR gene has been attempted, but this strategy is largely irreversible and cannot conduct real-time switch[26,27] (Supplementary Table 4 and Supplementary Note 5). In this study, a series of *in vivo* experiments have been conducted to demonstrate that the use of LiCAR can actually enhance the safety and reduce severe side effects associated with current anti-CD19 CAR T-cell therapy. Our wireless nano-optogenetic engineering provides a robust non-invasive approach to circumvent the limitations of conventional and chemical-based methods. Such NIR light-inducible approaches show multiple advances in terms of real-time spatial and temporal controllability, tunability, and non-invasiveness (Supplementary Note 5).

In sum, in conjunction with upconversion nanomaterials, LiCAR permits time- and location-specific CAR T cell-mediated antitumor activity via deep tissue penetrable NIR light *in vivo*. This hybrid strategy allows for the precise spatiotemporal regulation of the T cell-mediated immune response, as well as mitigating the side effects associated with existing FDA approved CAR T-cell therapy, such as “on-target, off-tumor” cytotoxicity and CRS. We anticipate that it can ultimately lead to the development of new generations of personalized nano-optogenetic immunotherapy, where the timing, location, and dosage of T cell-mediated therapeutic activity can be tailored to the patients’ needs. In addition, we believe that our nano-optogenetic platform will benefit the mechanistic dissection of CAR T-cell biology, which could serve as a unique tunable in vivo model to illuminate the kinetic and dynamic features of therapeutic T-cells and to define the safety threshold of anti-tumor immunity without eliciting detrimental side effects.

METHODS

Molecular cloning and plasmid construction

To construct plasmids encoding Component I (A0, C0, E0, and G0), gBlocks gene fragments were synthesized by Integrated DNA Technologies (Coralville, Lowa, USA) to generate the following cDNA sequences: CD8 signal peptide, Myc tag, anti-CD19 scFv, CD8-alpha transmembrane domain, hinge region, and 4-1BB. The synthetic block was inserted between the NheI-XhoI restriction sites into the mCerulean N1 vector (#27795; Addgene, Watertown, Massachusetts, USA). The optical dimerization components, including CIBN (#60553; Addgene), LOV2-ssrA (#60413; Addgene), CRY2PHR (#89877; Addgene), sspB (#60410;

Addgene) were first amplified via standard PCR with KOD Hot Start DNA polymerase (EMD Millipore, Burlington, Massachusetts, USA), and then inserted downstream of 4-1BB between the XhoI-XmaI sites. Two linkers, GSGSGEF and GSGSGSGS, were introduced before and after the dimerization modules, respectively. EGFP was amplified from the hRIP3-eGFP vector (#41387; Addgene) and then inserted between the AgeI-NotI restriction sites to replace mCerulean in the backbone vector. For Component I constructs, we generated versions with or without eGFP. To facilitate PM localization, Component I was further modified by inserting (i) a short ER export sequence to the N-terminus and (ii) an ER trafficking signal between the AgeI and MluI sites in front of eGFP in Constructs A0 and C0 (Extended Data Fig. 1a).

To construct plasmids encoding Component II (constructs B1.0/D1.0), we sequentially introduced the 4-1BB, sspB and human CD3ζ intracellular chain derived from gBlocks gene fragments and inserted them between the KpnI, EcoRI, HindIII, and BamHI restriction sites upstream of mCherry in the pmCherry2-N1 vector (#54517; Addgene). CRY2PHR (#89877; Addgene) was used to replace sspB to generate CRY2-based constructs. To create B2.0/D2.0 constructs, we rearranged the intracellular CAR components, and optical dimerization molecules with mCherry, 4-1BB, CD3ζ, and sspB/CRY2 were sequentially inserted into the BamHI, XhoI, EcoRI, and ApaI sites of pcDNA3.1 (+). The plasma membrane (PM)-tethered Component II constructs (B3/D3) were designed by fusing the CD8-alpha hinge and transmembrane domain upstream of the 4-1BB module in the reorganized CAR constructs (4-1BB, CD3ζ, mCherry, and CRY2/sspB). B4/D4 were generated by placing DAP10 (gBlock gene fragment) and the CD8-alpha transmembrane domain upstream of 4-1BB in the B1.0/D1.0 constructs between the XhoI and KpnI restriction sites. The defective LiCAR constructs (B5/D5) were generated from B4/D4 by removing the T cell-activating CD3ζ component. To reduce undesired nuclear accumulation, an NES sequence was inserted into the N-terminus of Component II constructs between the NheI and XhoI sites. Constructs D4.1 and D4.2 were generated by replacing sspB from construct D4 and D2 by sspB (R73Q) (#60420; Addgene) between the EcoRI/HindIII and EcoRI/ApaI sites, respectively. Constructs D4.3 and D4.4 were generated by introducing the point mutation A58V into sspB in the parental constructs D4 and D2 by using the QuikChange Lightning Multi Site-Directed Mutagenesis Kit (Agilent Technologies, Santa Clara, CA, USA) following the manufacturer's instructions.

For viral transduction, the pMSGV1 retroviral vector (#107227; Addgene) and MIGR1 (#27490; Addgene) were used as the backbones into which all the optimized CAR or LiCAR components were inserted between two modified restriction enzyme sites, HpaI and PacI. The helper plasmids including the gag/pol viral packaging vector (#14887; Addgene), a modified envelope vector encoding the amphotropic envelope glycoprotein RD114 (#17576; Addgene), and packaging vector pcl-Eco (#12371; Addgene) were acquired from Addgene.

Mammalian cell culture, transfection and fluorescence microscopy

An NFAT-dependent luciferase reporter (NFAT-Luc) Jurkat cell line was used to examine NFAT-dependent gene transcription as previously described[1]. Human cancer cell lines (K562 myelogenous leukemia cells (#CCL-243), Daudi (#CCL-213) and Raji cell lymphoblasts

(#CCL-86)) were purchased from the American Type Culture Collection (ATCC, Manassas, Virginia, USA), and cultured in Roswell Park Memorial Institute (RPMI 1640) medium with L-glutamine (#MT10040CV, Thermo Fisher Scientific, Waltham, Massachusetts, USA) supplemented with 10% FBS, 100 units/ml penicillin and 100 μg/mL streptomycin (Gibco, Big Cabin, Oklahoma, USA). B16-OVA and the B16-OVA mouse melanoma cell lines transduced with an amphotropic virus containing human CD19 (hCD19) (gifts from Dr. Anjana Rao, La Jolla Institute for Immunology) were maintained in Dulbecco's Modified Eagle Medium (DMEM) (#MT10013CV, Thermo Fisher Scientific) supplemented with 10% FBS, 100 units/ml penicillin and 100 μg/mL Streptomycin (Gibco). The CD19 level of each cell line was quantified by staining the cell surface with a monoclonal antibody against CD19 (APC-conjugated; #17-0199-42; dilution 1:200; eBioscience, San Diego, California, USA) in FACS buffer (PBS, 2% BSA, and 2 mM EDTA) at 4 °C for 30 min. The stained cells were washed three times with FACS buffer, and the levels of fluorescence protein were determined by using the LSRII flow cytometer (BD Biosciences, San Jose, California, USA). Cells were sampled at a medium flow rate, and at least 10,000 cells were counted for each condition. FACSDiva8.0 (BD Biosciences) and FlowJo software v10.5.3 (TreeStar, Ashland, Oregon, USA) were used to analyze the data (APC^+ cell populations).

HeLa cells from ATCC (#CCL-2) were maintained in Dulbecco's Modified Eagle Medium (DMEM) (#MT10013CV, Thermo Fisher Scientific) supplemented with 10% FBS, 100 units/ml penicillin and 100 μg/mL streptomycin (Gibco) at 37 °C in a humidified atmosphere under 5% CO_2. For confocal imaging, 10^5 cultured cells were seeded on 35 mm glass-bottom dishes. After 24 h, LiCAR components I (1000 ng) and II (600 ng) were co-transfected into HeLa cells using Lipofectamine 3000 (Life Technologies; Carlsbad, California, USA) according to the manufacturer’s instructions. Confocal imaging was performed at 24 h post-transfection by using an inverted Nikon Eclipse Ti-E microscope customized with Nikon A1R+ confocal laser sources (405/488/561/640 nm). A 488-nm laser was used to excite GFP, which also served as an internal light source for photo-stimulation in some cases, and a 561-nm laser was used to excite mCherry fluorescence. The cells were subjected to two dark-light cycles, in which each cycle had fifteen repetitions of 1-s stimulation and either 3-min of image acquisition for LOV2-based constructs or 6 minutes for CRY2-based constructs. At least four GFP- or mCherry-positive cells were selected to calculate the cytosolic fluorescence at selected areas before and after photo-stimulation (F/F_0). Image data analyses were performed using the Nikon NIS-Elements Analysis package (version 4.51.00) and Image J (NIH; version 1.51a) software.

Isolation and culture of primary human T cells

Peripheral blood mononuclear cells (PBMCs) were collected from blood samples of healthy blood donors through the Gulf Coast Regional Blood Center (Houston, Texas, USA) by density gradient centrifugation using the Ficoll-Paque Plus media (#GE17-1440-02; Sigma, St. Louis, Missouri, USA). The use of human blood samples was in accordance with the ethical standards of institutional guidelines on human cell research by the Institutional Review Board (IRB) of Texas A&M University. All obtained blood samples were anonymized and deidentified and are therefore eligible for an IRB waiver. PBMCs were washed three times with sterile PBS and resuspended at a concentration of 1 × 106

cells/ml in PBS supplemented with 2% BSA and 2 mM EDTA. CD8+ T cells from PBMCs were enriched by magnetic cell sorting, using negative selection kits (#130-096-495; Miltenyi Biotec, Auburn, California, USA). The purity of the $CD8^+$ cell populations was determined using flow cytometry by staining with APC-conjugated anti-human CD8 (#344721; Biolegend; dilution 1:200). $CD8^+$ T cells were cultured in RPMI L-glutamine medium supplemented with 10% FBS, 1X NEAA (non-essential amino acid medium; #1939940; Gibco), 1 mM sodium pyruvate (#13-115E; Lonza, Houston, Texas, USA), 10 mM HEPES (#15630-080; Gibco), 0.55 μM 2-mercaptoethanol (#21985023; Gibco), 100 units/ml penicillin, and 100 μg/mL streptomycin. Recombinant human IL-2 (#PHC0027; Gibco) was used at a final concentration of 100 IU/mL for culturing $CD8^+$ cells.

Isolation and culture of mouse T cells

Spleens were excised from 6 – 12-week-old C57BL/6 mice and put in 5 ml of FACS buffer. Each spleen was then transferred to a 100 μm cell strainer atop a 35 mm plate containing 2 ml of FACS buffer. The plunger of a small syringe was used to crush the spleen in the strainer. The cell suspension from the plate beneath was collected and briefly centrifuged. Red blood cells were removed from the cell pellets by resuspension in 1 ml of ACK lysis buffer (#10-548E; Lonza) for 1 minute. After that, AKC buffer was diluted by adding 9 ml FACS buffer. The cells were then harvested, washed one more time, and resuspended at a concentration of 1×10^6 cells/ml in FACS buffer. Mouse spleen $CD8^+$ T cells were enriched by magnetic cell sorting using negative selection kits (#130-104-075; Miltenyi Biotec). The purity of the $CD8^+$ cell populations was determined using flow cytometry by staining with anti-mouse CD8a eFluor 450 (#48-0081-82; dilution 1:200; eBioscience). Mouse $CD8^+$ T cells were cultured in TexMACS media (#130-097-196; Miltenyi Biotec) supplemented with 10% FBS, 100 units/ml penicillin, and 100 μg/mL streptomycin. 400 ng/mL anti-mouse CD3 (#50-139-2707, Fisher Scientific), 400 ng/mL anti-mouse CD28 (#50-562-020, Fisher Scientific), and 100 IU/mL recombinant mouse IL-2 (#PMC0025; Gibco) was freshly added to the medium each time used.

Viral transduction of Jurkat T cells and primary T cells

Retroviruses encoding the conventional CAR or engineered CARs were packaged in HEK293T cells (#CRL-3216; ATCC) transfected with the corresponding retroviral vector pMSGV1, the gag/pol viral packaging vectors (#14887; Addgene) and a modified vector encoding the amphotropic envelope glycoprotein RD114 (#17576; Addgene) using the iMFectin DNA Transfection Reagent (#I7200-101; Gendepot, Katy, Texas, USA). For mouse T cell transduction, the retroviruses were packed in Plate-E cells (#RV-101; Cell Biolabs, San Diego, California, USA) transfected with the packaging vector pcl-Eco (#12371; Addgene) and MIGR1-WT CAR, MIGR1-LiCAR, or MIGR1-defective CAR constructs. The supernatant containing packaged viruses was collected twice at 48 hours and 72 hours after transfection.

Cultured Jurkat T cells at a concentration of 10^5 cells/ml were co-incubated with 2 ml of the 0.45 μM filtered virus supernatant and 10 μg/ml of polybrene per well in a 12-well plate format. Plates containing cultured cells were centrifuged at 2000 x g for 2 hours at 32 °C and incubated 2 more hours at 37°C. The viral supernatant was removed and replaced with

fresh RPMI medium supplemented with 10% FBS, 100 units/ml penicillin and 100 μg/mL streptomycin. Cells were repeatedly transduced four times to yield a higher transduction efficiency.

For human primary T cells, the virus-containing supernatants were first concentrated using the Amicon Ultra-15 Centrifugal Filter (#UFC903024; Millipore Sigma, St. Louis, Missouri, USA). Before performing T cell transduction, human primary $CD8^+$ T cells were activated for 48 hours using the Dynabeads Human T-Activator CD3/CD28 system (#11132D; Thermo Fisher Scientific) at a bead-to-cell ratio of 1:1. Retroviral transduction of primary T cells was performed by mixing concentrated viruses and RetroNectin (#T100B; Takara Bio, Mountain View, California, USA) with T cells according to the manufacturer's instructions.

For mouse primary T cells, $CD8^+$ T cells were activated overnight in IgG (H+L) goat anti-Hamster (#PI31115, Fisher Scientific)-coated plates (20 μg/ml) and soluble anti-mouse CD3 (#50-139-2707, Fisher Scientific) and anti-mouse CD28 (#50-562-020, Fisher Scientific) in mouse T cell culture medium. Mouse T cells were transduced with 2 ml of 0.45-μM filtered virus supernatant and 10 μg/ml of polybrene per well in a 12-well plate. Both human and mouse primary T cells were transduced by centrifugation two times to achieve efficient transduction. Expression of transgenes was confirmed by detecting fluorescent reporters using an LSRII flow cytometer (BD Biosciences).

In Vitro quantification of NFAT-luciferase (NFAT-Luc) reporter activity of Jurkat-Luc T cells

Jurkat T cells expressing conventional CARs, LiCAR, or defective LiCAR (10^5 cells/well) were co-cultured with cognate CD19-positive Raji cells or non-cognate CD19-negative K562 cells at indicated effector T cell: target cell (E/T) ratios or at the ratio of 1:3 in a 96-well flat-bottom microplate (#E17073EF; Greiner Bio-one, Monroe, North Carolina, USA). Plates with cells were incubated at 37 °C in a humidified atmosphere under 5% CO_2 and either kept in the dark or subjected to photostimulation (470 nm at a power density of 40 mW/cm^2) for 1 to 25 minutes and then with pulsed blue light (10-30 sec ON, 100 sec OFF) for up to 8 hours. Cell pellets were then harvested, and luciferase activity was assayed by using the Bright-Glo Luciferase Assay System (Promega, Fitchburg, Wisconsin, USA) on the Cytation 5 luminescence microplate reader (BioTek, Winooski, Vermont, USA). Data plots were generated by using the Prism version 8.0.0 software (GraphPad, San Diego, California, USA).

ELISA measurements of cytokine production

Jurkat cells expressing conventional CARs, LiCAR, or defective LiCAR (10^5 cells/well) were mixed with either $CD19^+$ Raji cells or $CD19^-$ K562 cells at an E/T ratio of 1:3, while mouse CD8 T cells transduced with viruses encoding CAR constructs were co-cultured with B16-OVA or B16-OVA-hCD19 at the indicated E:T ratios. The cells were incubated in the dark or exposed to blue light (470 nm at a power density of 40 mW/cm^2) continuously for 1 to 25 minutes and then to pulsed blue light (10-30 sec ON, 100 sec OFF) for up to 12 hours. Cell supernatants were collected and analyzed with BD OptEIA Human IL-2 ELISA Set (#555190; BD Biosciences, San Jose, California, USA) or mouse IFN-γ ELISA set (#88-7314-22, Invitrogen, Carlsbad, California, USA) according to the manufacturer's

instructions. Briefly, one day before collecting cell supernatant, a 96-well flat-bottom microplate (#E17073HT; Greiner Bio-one) was coated with human anti-IL-2 or mouse anti-IFN-γ antibody (at a dilution of 1:1000 in PBS) at 4°C overnight. On day 2, the plate was washed with 200 μl PBS/0.05% Tween 20 and then blocked with 1% BSA/PBS for 2 h at room temperature. Cell supernatants were diluted 1:10 in 1% BSA/PBS before being added into the plate wells. A series of cytokine standard dilutions were applied to obtain a standard curve. The plate was then incubated at 4°C overnight. The next day, 100 μl of biotin-conjugated detection antibody (1:1000 in 1%BSA/PBS) was added and incubated with cell supernatants for 1 hour at RT. The plate was then washed and incubated with HRP streptavidin (1:3000 in 1% BSA/PBS) at RT for 30 min. After a final wash, each well was incubated with 100 μl of the tetramethyl-benzidine substrate solution (#34028, Thermo Fisher Scientific). 50 μl of 2.5N H_2SO4 (#35348, Honeywell Fluka, Mexico City, Mexico, USA) was added to each well to stop the reaction. For mIL-6 quantification, mouse blood sera were collected and analyzed with an IL-6 Mouse ELISA Kit (#KMC0062, Invitrogen, Carlsbad, California, USA) according to the manufacturer's instructions. The absorbance of each well was measured at 450 nm using the Cytation 5 luminescence microplate reader (BioTek). The concentration of samples was calculated based on the standard curve, and data were replotted with the Prism software (GraphPad).

Flow cytometry analysis on CD69 surface expression in T cells

Jurkat T cells transduced with conventional CARs, LiCAR, or defective LiCAR (10^5 cells/well) were co-cultured with either CD19-negative (K562) or CD19-positive (Daudi/Raji) target tumor cells at a ratio of 1:3 in 96-well flat-bottom microplates (#E17073EF; Greiner Bio-one). The light stimulation was given for 20 min at a power density of 40 mW/cm^2 and then with pulsed blue light (10 sec ON, 60 sec OFF) for 10 h. After incubation, cells were washed and stained with an Alexa Fluor 700 conjugated anti-human CD69 antibody (#310922; dilution 1:200; Biolegend) at 4°C for 30 min in FACS buffer. Cells were washed three times in PBS and then analyzed by a BD LSRII cytometer (BD Biosciences). Data were analyzed using the FACSDiva8.0 (BD Biosciences) and FlowJo software v10.5.3 (TreeStar).

Tumor cell killing assays

Human $CD8^+$ T cells expressing conventional CARs, LiCAR, or defective LiCAR and the cognate $CD19^+$ Daudi target cells used in this assay were maintained with a viability of over 97%. The effector T cells were co-cultured with target cells at an E/T ratio ranging from 1:1 to 1:3 using CD8 T cell medium in 96-well plates. Cells were evenly distributed into two plates, with one plate shielded from light as the control in the dark state and the other subjected to photostimulation (470 nm, power density of 40 mW/cm^2) for 20 min every 2 hours for the first 8 h, followed by pulsed blue light (10 s ON, 60 s OFF) for 16 h.

The mixture of human $CD8^+$ T and Daudi cells was then harvested and stained with SYTOX Blue dye (#S11348; Invitrogen) at a final concentration of 100 nM for 15 min at 4 °C in FACS buffer. The cells were then washed twice and resuspended in FACS buffer and subjected to flow cytometry analysis by using a BD LSRII cytometer or a BD FACSAria

sorter (BD Biosciences). The FlowJo software v10.5.3 (TreeStar) was used to calculate the death rate of targeted B cells (gated on GFP^-, mCh^-, and $SYTOX^+$).

For time-lapse fluorescence microscopy, engineered $CD8^+$ T-cells were immobilized on 35-mm glass-bottom dishes by using 0.1 mg/ml poly-L-lysine (#2840311; EMD Millipore). $CD19^+$ Daudi cells and SYTOX Blue (100 nM) were subsequently added to the well in T cell culture media. Fluorescence images were acquired at 37 °C and 5% CO_2 in a humidified atmosphere at 40x magnification. The time-lapse recording lasted for about 5 hours at an interval of 2 min under blue light illumination (blue LED at 470 nm with a power density of 40 mW/cm^2). The tumor cell killing activity of LiCAR T-cells (GFP^+, mCh^+) was monitored by their engagement with Daudi cells to induce target cell death, which was made visible by the SYTOX Blue nucleic acid staining dye.

For *ex vivo* murine melanoma cells killing assay, B16-OVA-hCD19 cells were seeded onto 96-well glass bottom plates (#655892; Greiner Bio-one) with 10^3 cells per well. Cells were incubated overnight for attachment. Mouse $CD8^+$ T cells expressing CAR constructs were added to pre-seeded B16-OVA-hCD19 cells at the indicated E/T ratios. One plate was kept in the dark and another plate was subjected to blue light illumination (470 nm with a power density of 40 mW/cm^2) for 20 min every 2 hours for the first 8 h, followed by pulsed blue light (10 s ON, 60 s OFF) for 16 h. The plates were then washed three times with PBS to remove unattached T cells and dead B16-OVA-hCD19 cells. The surviving B16-OVA-hCD19cells, which remained attached to the plate bottom, were visualized by DAPI staining. A high-content confocal imaging system (In cell Analyzer 6000; GE Healthcare Life Sciences, Chicago, Illinois, USA) was used to capture the images of each well. Cells numbers were quantified using the IN Cell Developer Toolbox version 1.9 (GE Healthcare). Data plots were generated by using Prism version 8.0.0 software (GraphPad).

Synthesis of β-$NaYbF_4$:0.5%Tm@$NaYF_4$ Core-shell UCNPs

The β-$NaYbF_4$:0.5%Tm@$NaYF_4$ UCNPs were prepared by a three-step thermolysis method. In the first step, CF3COONa (0.50 mmol), Yb(CF3COO)3 (0.4975 mmol) and Tm(CF3COO)3 (0.0025 mmol) precursors were mixed with oleic acid (5 mmol), oleyamine (5 mmol), and 1-octadecene (10 mmol) in a two-neck round bottom flask. The mixture was heated to 110 °C to form a transparent solution followed by 10 min of degassing. Then the mixture was heated to 300 °C at a rate of 15 °C/min under dry argon flow, and maintained at 300 °C for 30 min to form the α-$NaYbF_4$:0.5%Tm intermediate UCNPs. After the mixture cooled down to room temperature, the α-$NaYbF_4$:0.5%Tm intermediate UCNPs were collected by centrifugal washing with excessive ethanol (7500 x g, 30 min). In the second step, the α-$NaYbF_4$:0.5%Tm intermediate UCNPs were redispersed into oleic acid (10 mmol) and 1-octadecene (10 mmol) together with CF3COONa (0.5 mmol) in a new two-neck round bottom flask. After degassing at 110 °C for 10 min, this flask was heated to 325 °C at a rate of 15 °C/min under dry argon flow and maintained at 325 °C for 30 min to complete the phase transfer from α to β. After the mixture cooled to room temperature, the β-$NaYbF_4$:0.5%Tm core UCNPs were collected by precipitation with an equal volume of ethanol followed by centrifugation (7500 x g, 30 min). The β-$NaYbF_4$:0.5%Tm core UCNPs were stored in hexane (10 mL). In the third step, the as-synthesized β-$NaYbF_4$:0.5%Tm core

UCNPs served as cores for the epitaxial growth of core-shell UCNPs. Typically, a hexane stock solution of β-$NaYbF_4$:0.5%Tm core UCNPs was transferred into a two-neck round bottom flask, and the hexane was sequentially evaporated by heating. CF_3COONa (0.25 mmol) and $Y(CF_3COO)_3$ (0.25 mmol) were introduced as UCNP shell precursors with oleic acid (10 mmol) and 1-octadecene (10 mmol). After 10 min of degassing at 110 °C, the flask was heated to 325 °C at a rate of 15 °C/min under dry argon flow, and maintained at 325 °C for 30 min to complete the shell crystal growth. After the mixture cooled to room temperature, the β-$NaYbF_4$:0.5%Tm@$NaYF_4$ core-shell UCNPs were collected by precipitation with an equal volume of ethanol followed by centrifugation (7500g, 30 min). β-$NaYbF_4$:0.5%Tm@$NaYF_4$ core-shell UCNPs were stored in hexane (10 mL). The control sample of β-$NaYF_4$:30%Yb,0.5%Tm@$NaYF_4$ core-shell UCNPs were synthesized similarly, except for changing the amount of $Ln(CF_3COO)_3$ according to the stoichiometric ratio.

Synthesis of silica coated core-shell UCNPs

The silica shell was coated onto the core-shell UCNPs via a modified Stober method. In a typical process, 4 mL of the core-shell UCNP hexane solution was added to 21 mL hexane in a 50 mL one-neck round bottom flask. 1.5 mL of Igepal CO-520 was added to the solution which was kept in a water bath while sonicated for 2 minutes. 160 μL of ammonia was added to the solution. After 30 minutes of stirring, 80 μL of TEOS (Tetraethoxysilane) was added to the solution. After 2 days of stirring, the silica-coated core-shell UCNPs were collected by precipitation with an equal volume of ethanol, followed by centrifugation (7500 x g, 30 min) for 3 times. This silica-coated core-shell UCNPs were stored in water (20 mL).

Synthesis of streptavidin-conjugated UCNPs (Stv-UCNPs)

For intravenous administration, we used ~30 nm spherical β-NaYF4:30%Yb,0.5%Tm@NaYF4 core-shell UCNPs and conjugated them with streptavidin following our previously optimized protocols[1]. In a typical process, 1 ml of UCNPs in hexane were added into 5 ml dimethylformamide (DMF) solution containing 0.20 g nitrosonium tetrafluoroborate (NOBF4). After stirring the mixture for 2 hours, the mixture stood still for 5 min. The UCNPs capped by BF4-dispersed at the bottom DMF layer were taken out and precipitated with isopropanol (5 ml) by centrifuging at 11000 x g for 15 min. The washing steps were repeated to two additional cycles with 5 ml of isopropanol and 5 ml DMF. Next, the UCNPs were dispersed in 5 ml DMF solution containing 50 mg poly(acrylic acid) (PAA). The PAA was coated onto UCNPs after overnight incubation with constant stirring and washed three cycles by deionized (DI) water and centrifugation at 11000 x g for 15 min. The UCNPs-PAA were dispersed in 5 ml DI water and activated by EDC (1-Ethyl-3-(3-dimethylaminopropyl)-carbodiimide, 50 mg) and NHS (N-Hydroxysuccinimide, 10 mg) to form succinimidyl ester for 2 hours, followed by washing with DI water and centrifugation at 11000 x g for 15 min. After redispersing the UCNPs in 5 ml DI water, 150 μg streptavidin was added and the mixture was stirred at room temperature for 4 additional hours. The streptavidin-UCNPs (Stv-UCNPs) were collected, washed three times by DI water and centrifuged at 11000 x g for 15 min. Stv-UCNPs were suspended in PBS at the concentration of 1.5 mg/ml for further functional studies.

T cell biotinylation and coupling with Stv-UCNPs

Jurkat or human $CD8^+$ T-cells expressing WT CAR or LiCAR, as well as Jurkat T cells as control, were washed three times in cold PBS to deplete residual free amine-containing buffers. Cells were then suspended at a concentration of 2.5 x 10^7 cells/ml. Subsequently, 200 ul of 10 mM EZ-Link Sulfo-NHS-Biotin (#A39256, Thermo Fisher Scientific) was added to 1 ml of cell suspension. The mixture was incubated at 4°C for 30 minutes. The cells were washed three times with 100 mM glycine in PBS. Biotinylated cells were further incubated with APC-conjugated streptavidin (#405207, BioLegend) to evaluate the biotinylation efficiency by flow cytometry. To prepare for Stv-UCNP-CAR T-cell mixture, 0.1 ml Stv-UCNPs (1.5 mg/ml) was mixed with 1 x 10^7 biotinylated $hCD8^+$ T-cells expressing WT CAR or LiCAR, and then incubated at 4°C for 30 min. Unbound St-UCNPs were washed away by centrifuging the mixture at 700 x g for 5 minutes. UCNP-coupled CAR T-cells were re-suspended in PBS and administered into mice via tail vein injection.

Cryosection and immunostaining of tumor samples

Tumor tissues were fixed in 4% paraformaldehyde overnight at 4 °C. After washing with PBS twice, tissues were placed in plastic Seal'N Freeze cryo-embedding molds containing Optimal Cutting Temperature (OCT) compound (Sakura Finetek, CA, USA). Tissues were then shock-frozen in a dry ice ethanol bath and kept at −80 °C. 10 μm cryosections were prepared using cryostat (#CM3050S, Leica, Wetzlar, Germany) and were stored at −80°C for further use. Prior to immunostaining, cryosections were washed with PBS twice at room temperature. Nuclei were stained with 0.5 ng/μl DAPI for 10 minutes. After washing with PBS twice, ProLong Diamond Antifade Mountant (Thermo Fisher Scientific) was added to fix the cover glass in place and prevent fluorescence fading.

Cell proliferation assay

Cell proliferation was quantified using the WST-1 colorimetric assay (#05015944001; Sigma) according to the manufacturer's instructions. Briefly, on day 1, B16-OVA and B16-OVA-hCD19 cells were seeded in a 96-well plate (10^3 cells per well) in 200 μl of DMEM medium supplemented with 10% FBS, 100 unit/ml penicillin and 100 μg/mL streptomycin. After incubation for the indicated times, 20 μl of WST-1 was added to each well and incubated at 37°C, 5% CO_2 for 2 h. The cell plates were shaken for 1 min on a shaker. The absorbance of each well against a background control (medium with WST-1 only) was measured at 450 nm using a Cytation 5 luminescence microplate reader (BioTek). Data plots were generated by using Prism version 8.0.0 software (GraphPad).

Syngeneic mouse model of melanoma

All animal studies were approved by the Institutional Animal Care and Use Committee of Texas A&M University Institute of Biosciences and Technology with the maximum allowable tumor size of <20 mm in diameter for each mouse. On day 0, 6-12-week-old C57BL/6J mice (either sex) were inoculated intradermally with 2.5-5 x 10^5 B16-OVA and B16-OVA-hCD19 or B16-OVA-mCD19 cells depending on each experiment. When the tumors became visible, their sizes were measured with a digital caliper every day, and the tumor area was calculated in square millimeters (length x width). The tumors were allowed

to grow for 8 additional days after inoculation. On day 9, 2 x 10^6 mouse CD8 T cells expressing CAR constructs and 150 μg of UCNP were co-injected into each tumor. From day 10, LiCAR-treated mice (hLiCAR or mLiCAR) were subjected to pulsed near-infrared light treatment (980 nm at a power density of 250 mW/cm^2; pulse: 20 sec ON, 5 minutes OFF for 2 hours per day). On day 16 to 19, tumors were collected from euthanized mice. For the analysis of hLiCAR T cells residing within the tumors, tumors were collected, perfused in PBS, cut into small pieces and enzymatically digested with 5 ug/ml of Liberase TL (#298569; Roche, Basel, Switzerland) for 1 hour at 37°C. Tumor cells were then filtered by using a 100 μm cell strainer. Cells were washed twice in PBS to remove cell debris and resuspended in FACS buffer. The number of adoptively transferred hLiCAR T cells was determined by detecting hLiCAR fluorescence protein using the LSRII flow cytometer (BD Biosciences). FACSDiva8.0 (BD Biosciences) and FlowJo software v10.5.3 (TreeStar, Ashland, Oregon, USA) were used to analyze the data (gated on the GFP^+/mCh^+ population). For the analysis of hLiCAR T-cells residing within the spleen or blood, spleen cells were isolated by crushing the spleen on the strainer as described above while blood cells were collected from the retro-orbital sinus by glass capillary from anesthetized mice. Spleen and blood cells were then treated with ACK lysis buffer (#10-548E; Lonza) to remove red blood cells. The spleen and blood cells were washed twice before performing flow cytometry analyses.

Mouse model of lymphoma and systemic delivery of engineered CAR T-cells

On day 0, 8-12-week-old C.B-*Igh*-1b/GbmsTac-*Prkdc*^{scid}-*Lyst*^{bg} N7 mice (Taconic Biosciences, New York, USA) were inoculated intradermally on both flanks with the mixture of 1.5 x 10^5 $CD19^+$ Raji cells and Matrigel matrix (#354248, Corning, New York, USA) at a volume ratio of 1:1 (total volume 100 μl per side). When the tumors became visible, their sizes were measured with a digital caliper every 1-2 days, and the tumor area was calculated in square millimeters (length x width). After 6-7 days, depending on the experimental setup, 150 μg of UCNPs or PBS (control) were intratumorally (*i.t.*) injected into each tumor. Subsequently, 1 x 10^7 LiCAR-$hCD8^+$ T cells were systematically injected via tail vein injection (*i.v.*) for two doses (one time per week). In a second systemic administration method using Stv-UCNP-LiCAR T-cells, 1 x 10^7 engineered T cells were injected via tail vein to Raji lymphoma mouse models with two weekly doses. All treated mice were subjected to pulsed NIR light stimulation for 13 to 14 days (980 nm at a power density of 250 mW/cm^2; 20 sec ON + 5 minutes OFF; 2 h/day; NIR groups), or shielded from the NIR light source (dark groups). On day 20 or 21, mice were euthanized for tumor isolation and phenotypic analyses.

Mouse B cell quantification

WT mCAR T or mLiCAR T-cells/UCNPs were implanted into C57BL/6 mice bearing B16-OVA or B16-OVA-mCD19 tumors (both subcutaneous and intraperitoneal injection). mLiCAR-transferred mice were subjected to pulsed near-infrared light treatment (980 nm at a power density of 250 mW/cm^2; pulse: 20 sec ON, 5 minutes OFF for 2 hours per day). On day 0 and day 3, 200 μl of blood was collected from the retro-orbital sinus by glass capillary or from tail-clip from anesthetized mice. RBC was then removed by using ACK lysis buffer (#10-548E; Lonza). Total cell counts in peripheral blood were determined by

using a TC20 Automated Cell Counter (Biorad, CA, USA). The percentage of B cells in the total cell population was quantified using the LSRII flow cytometer (BD Biosciences) after staining cells with a monoclonal antibody against mCD19 (APC-conjugated; #17-0193-82; eBioscience) in FACS buffer at 4 °C for 30 min. The stained cells were washed three times with FACS buffer and were sampled at a medium flow rate with 10,000 cells counted. FACSDiva8.0 (BD Biosciences) and FlowJo software v10.5.3 (TreeStar, Ashland, Oregon, USA) were used to analyze the data (APC^+ cell populations). Based on the percentage of B cells in the cell population, we calculate the amount of B cells per μl blood.

Xenogeneic models using SCID-Beige mice to assess CRS

We used a recently well-adopted murine model using SCID-Beige mice to evaluate CRS in vivo[2]. Briefly, on day 0, $3x10^6$ Raji cells were intraperitoneally injected into 6- to 8-week-old female C.B-*Igh*-1b/GbmsTac-*Prkdc*^{scid}-*Lyst*^{bg} N7 mice (Taconic Biosciences, New York, USA). After 3 weeks, mice were divided into three groups: one group was injected intraperitoneally with 3 x 10^7 WT CAR-expressing CD8 T-cells, while another group was injected with 3 x 10^7 LiCAR-expressing CD8 T cells. The control group was treated with PBS only. 3 days after injection, LiCAR-transferred mice were subjected to pulsed near-infrared light treatment (980 nm at a power density of 250 mW/cm^2; pulse: 20 sec ON, 5 minutes OFF for 2 hours per day). All the mice were weighed every day to evaluate the weight change. On day 0 and day 3, blood cells were collected from the retro-orbital sinus by glass capillary or by tail-clip from anesthetized mice. Blood was left to clot for 30 min at room temperature and then centrifuged 6000 x g at 4°C for 10 min. Serum was collected and kept frozen at −80°C until analysis. mIL-6 in the serum was detected using ELISA (#KMC0061, Invitrogen) following the manufacturer's instructions.

Element analysis of the UCNP distribution in mouse tissues

Element mapping was performed in the Electron Microscopy Facility at the University of Massachusetts Medical School. Dissected mouse tissues were fixed by immersion in 4% paraformaldehyde for 2 days at 4 °C and then kept frozen. After thawing the tissues, a second fixation was performed with 2.5% glutaraldehyde in 0.1.M Na Cacodylate buffer (ph 7.2) for 30 min at room temperature. The fixed samples were then washed three times in the same fixation buffer. Following the third wash, the samples were dehydrated through a graded series of ethanol (10, 30, 50, 70, 85, 95% for 20 min each) to three changes of 100% ethanol, and then they underwent critical point drying in liquid CO_2. The dried mouse tissues were then cut to expose the inside, and they were mounted onto aluminum stubs with carbon tape making sure that the exposed surfaces were facing up. All the samples were then carbon coated with 3 nm of carbon to ensure conductivity. The specimens were examined using an FEI Quanta 200 FEG MK II scanning electron microscope at 15 Kv accelerating voltage under two modalities, secondary electron and backscattered imaging. The samples were also examined using an EDS system (Oxford Link Inca 350 x-ray spectrometer) to determine the element distributions in the tissues. The element spectrum, element mapping, and atomic ratio of each element were presented as the raw data obtained in the INCA EDS system without further manipulation.

Cytotoxicity assessment of UCNPs

B16-OVA-hCD19 cells were cultured in Dulbecco's modified Eagle's medium (DMEM) containing 10% fetal bovine serum (FBS), 100 μg/ml streptomycin and 100 U/ml penicillin at 37 °C in a humidified incubator containing 5% CO2 and 95% air. The medium was replenished every other day and the cells were subcultured after reaching confluence. Cell viability was examined by using a well-established MTT assay. In brief, B16-OVA-hCD19 cells were plated in a 96-well plate. After 12 h, the nanoparticles were added at different concentrations (0, 20, 40, 60, 80, 100 μg mL^{-1}). The cells were incubated another 24 h under 5 % CO2 at 37°C. MTT solution (5.0 mg mL–1, 50 μL) was added to every well and left for 4 h. The old cell culture medium was removed carefully and 200 μL DMSO was added to every well. A microplate reader (Bio-Rad) was used to record the absorption at 595 nm. Cell viability (%) = OD value test/OD value control × 100 %.

In vivo assessment of potential UCNP toxicity

For histological analysis, on the 1st, 7th and 14th day after injection of UCNPs (1 mg/ml, 150 μL), mice were sacrificed and major organs (heart, liver, spleen, lung, kidney, and tumor) were dissected for H&E staining. Mice injected with 150 μl PBS were used as the control. In parallel, before the mice were euthanatized, blood samples (approximately 0.5 ml) were collected for blood panel analyses and blood chemistry tests.

Flow cytometry analysis of macrophages

To quantify the population of macrophages within tumor sites or spleens, tumor tissue or spleens were minced into small pieces, treated with 1 mg/ml collagenase I (Gibco) for 1 h at 37 °C and grounded using the rubber end of a 10-ml syringe (BD Biosciences). Cells were filtered through nylon mesh filters (Corning, cell strainer, 70 μm nylon). The single cells were collected by centrifugation (800 × g, 5 min), and blood cells in the tumor tissue were eliminated by cold NH_4Cl lysis. The cell suspensions were washed in cold PBS containing 2 % FBS. The dispersed cells were stained with fluorescence-labeled antibodies FITC-anti-F4/80 (total macrophages) and APC-anti-CD86 (M1 macrophages) or PE/Cy7-anti-CD206 (M2 macrophages) following the manufacturer's instructions. All antibodies were diluted 200 times. Flow cytometric analyses were performed on an LSRFortessa (BD Biosciences) and analyzed using FlowJo Software (Tree Star).

In vivo evaluation of UCNP stability

150 μL UCNPs (1mg/ml) were injected into the tumors in tumor-bearing mice or the leg muscles of healthy mice. On the 1st, 7th, 14th and 28th day after UCNP injection, mice were sacrificed, and the UCNP-injected tumor or muscle was isolated and fixed with 4% paraformaldehyde (PFA)/0.25% glutaraldehyde in 0.1 M sodium phosphate buffer (PB) overnight. After several washes in 0.1 M cacodylate buffer (pH 7.4), sections were postfixed with 1% osmium tetroxide (Sigma) in 0.1 M cacodylate buffer for 1 h. After six washes with water for 1 h each and dehydration through a graded ethanol series of 10%, 30%, 50%, 70%, 85%, 95% and 100% EtOH (10 min each for 10%-70%, 20 min each for 85%, 30 min each for 95% and 100% (three times)). UCNP-injected tumor or muscle was treated with propylene oxide for 10 min twice and then immersed in freshly prepared 50% (v/v)

Durcupan resin in propylene oxide overnight for resin infiltration (Sigma). UCNP-injected tumor or muscle was then immersed in freshly prepared Durcupan resin for six times, 1 hour each. Sections were then transferred to freshly prepared Durcupan resin contained in a tube and left in a 60°C oven for 2 days for resin curing. The UCNP-injected tumor/muscle was excised out from the flat-embedded sections and glued onto a resin block for ultrathin sectioning. 70 nm ultrathin sections were cut with a diamond knife (Diatome), collected in formvar-coated single-slot copper grid and briefly counterstained with 2% uranyl acetate in 50% ethanol and 0.4 % lead citrate. Sections were observed under electron microscope (Philips CM10 Electron Microscope) at 100 KeV accelerating voltage. The sample preparation and imaging were performed in the Electron Microscopy Facility at the University of Massachusetts Medical School.

Extended Data

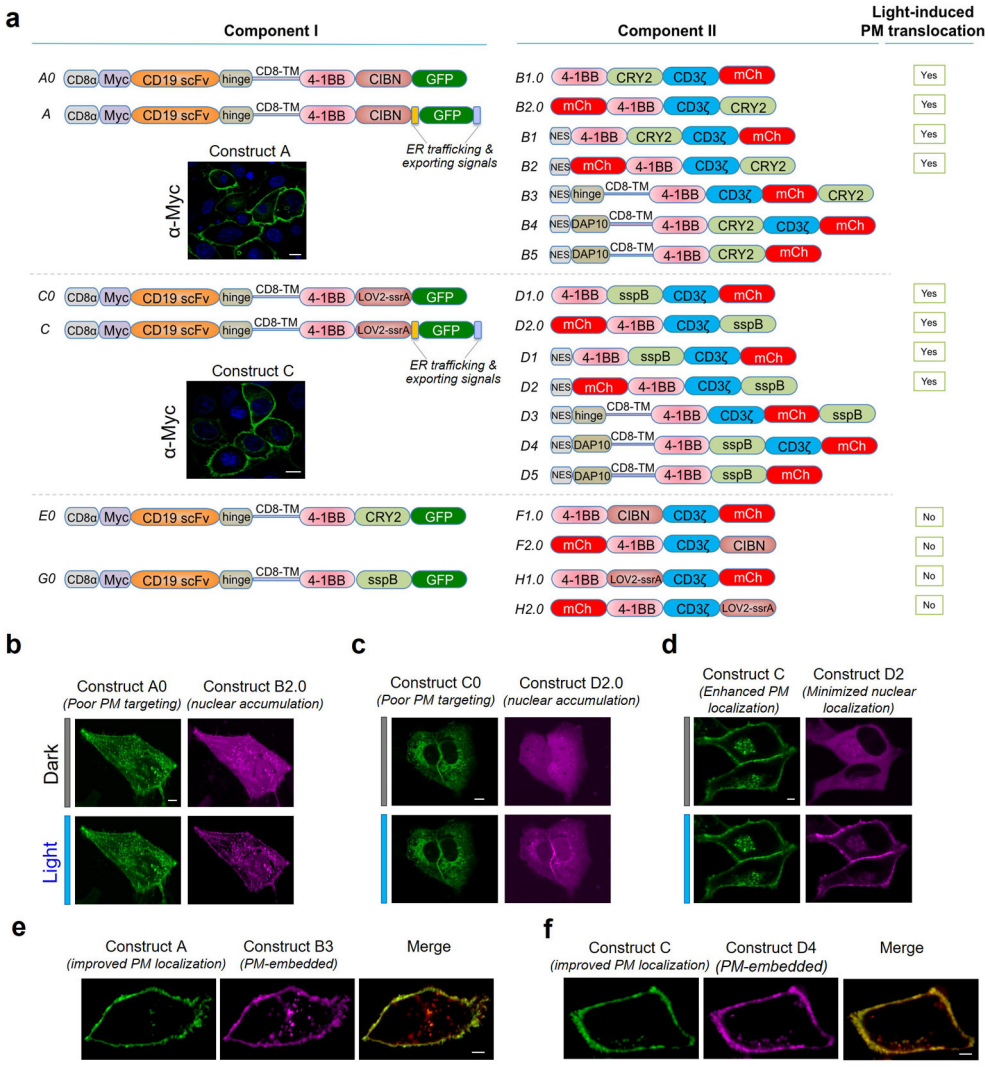

Extended Data Fig. 1. Design and screening of CRY2- and LOV2-based LiCARs.

a, Constructs used to screen and optimize the designed LiCARs (Components I+II). The inset showed confocal images of HeLa cells expressing the PM-embedded constructs A or C (without fluorescent tag) after non-permeabilized immunostaining with an anti-Myc antibody. When Component II was expressed as a cytosolic protein, we also monitored light-inducible cytosol-to- PM translocation to confirm the photo-responsiveness of the optical dimerizer. Scale bar, 5 μm.

b-d, Confocal images of HeLa cells expressing the indicated components before and after light illumination. The introduction of ER trafficking/export signals in Component I significantly improved PM targeting; whereas the addition of NES to Component II substantially reduced nuclear accumulation (**b/c** vs **d**). Four images for each combination were taken. Scale bar, 5 μm.

e-f, Confocal images of HeLa cells co-expressing constructs A+B3 or C+D4. Note that B3 and D4 contained the CD8 transmembrane domain (TM) and were thus embedded in the plasma membrane. Four images for each combination were taken. Scale bar, 5 μm.

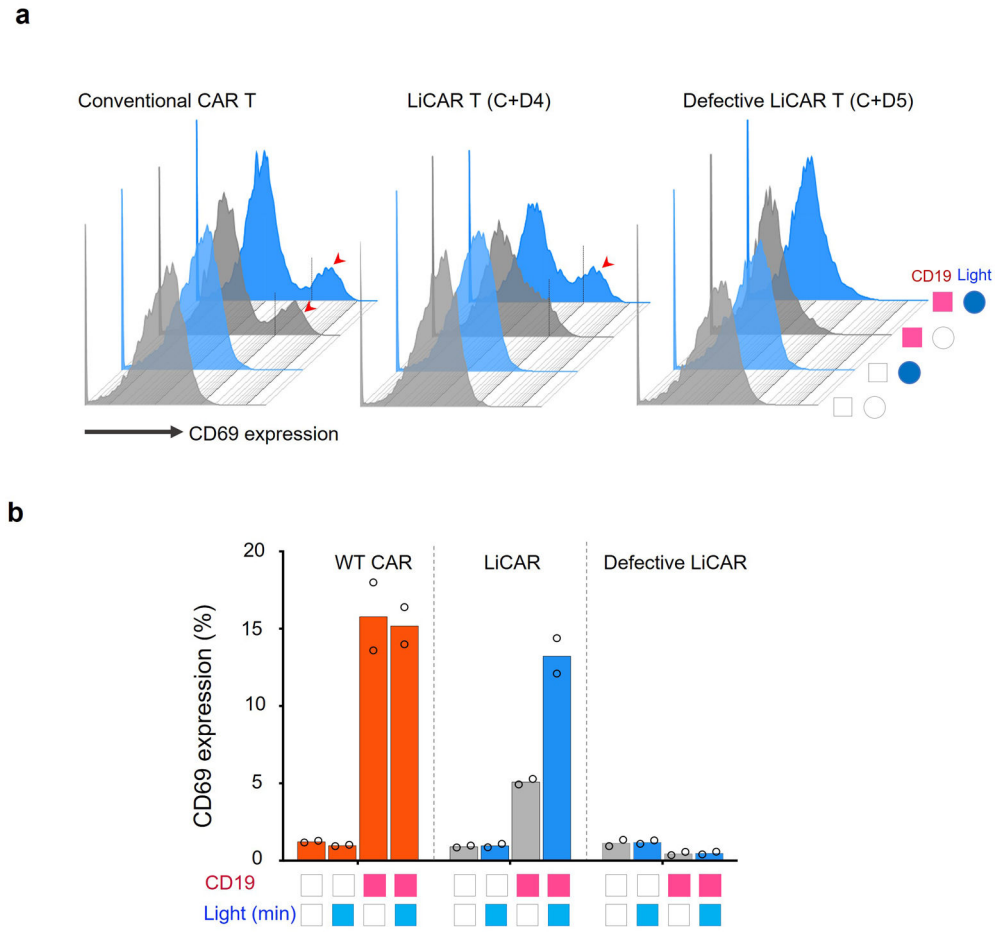

Extended Data Fig. 2. Early T cell activation reported by cell surface expression of CD69

a, Quantification of the CD69 expression level in Jurkat T cells expressing WT CAR, defective LiCAR (C+D5 lacking the CD3 subunit), or LiCAR (C+D4) before (open box) and after light illumination (blue box; 20 min and then 10 h with the pulse of 10 s ON

+ 60 s OFF). Cells were co-incubated with hCD19- negative K562 cells (open box) or hCD19-positive Raji cells (red box).

b, Quantification of CD69 expression in Jurkat T cells co-cultured with hCD19-negative K562 (open box) or hCD19-positive Raji cells (red box). n = 2 independent biological replicates (mean ± range).

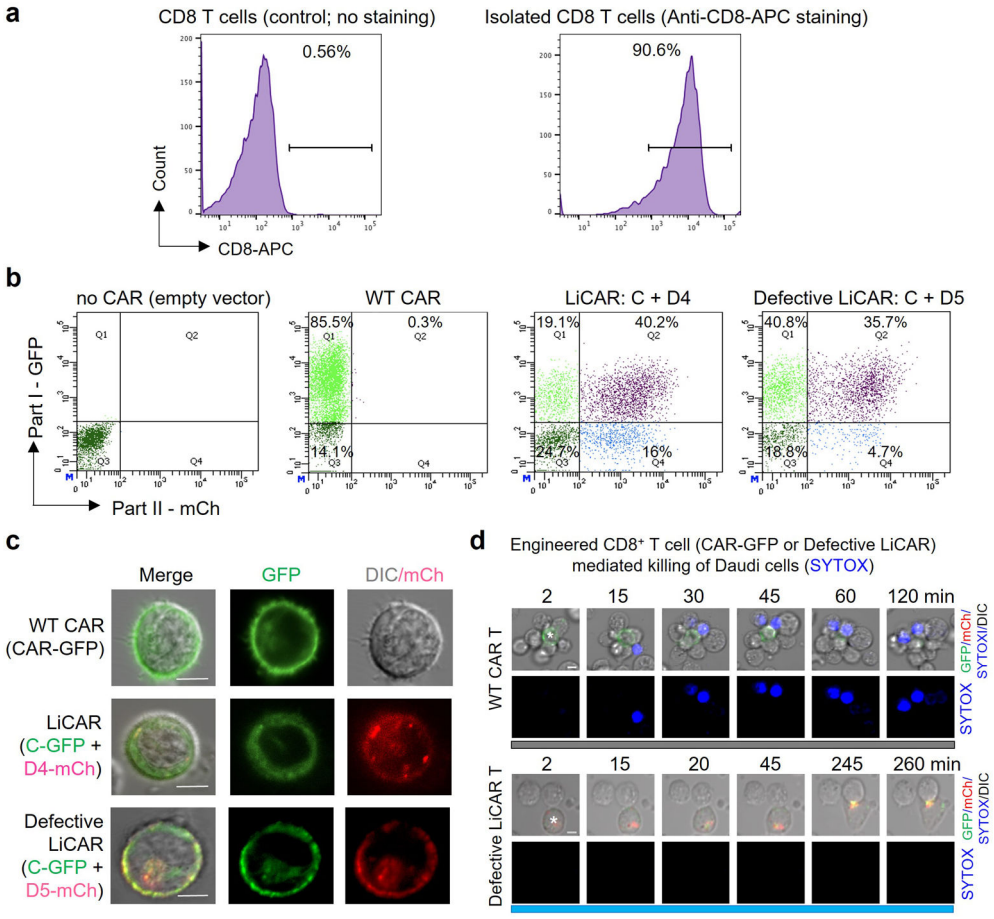

Extended Data Fig. 3. Expression of engineered CARs in human primary CD8$^+$ T cells

a, Evaluation of the purity of CD8$^+$ T cells isolated from PBMCs of healthy donors. Isolated T cells were stained with anti-CD8-APC. Non-stained CD8$^+$ T cells were used as negative control to aid the gating of cell populations.

b, Quantification of WT CAR (GFP-tagged), LiCAR (C-GFP + D4-mCh) or defective LiCAR (C-GFP + D5-mCh) expression in human CD8$^+$ T cells. GFP-positive (for the WT CAR group) or double positive cells (for the LiCAR and the defective LiCAR groups) were used for functional assays.

c, Confocal images of human CD8+ T-cells transduced with WT CAR (green, top panel) or the indicated CAR components (C-GFP, green; or D4/D5-mCherry, red; middle and bottom panels). Three images per group were taken. Scale bar, 10 μm.

d, Time-lapse imaging of tumor cells (Daudi) co-cultured with human CD8$^+$ T cells (asterisk) expressing either WT CAR (GFP-tagged, top) in the dark or defective LiCAR

(C-GFP+D5-mCh, bottom) exposed to blue light. Dying cells were indicated by SYTOX blue staining. Scale bar, 5 μm. Also see Supplementary Videos 3-4.

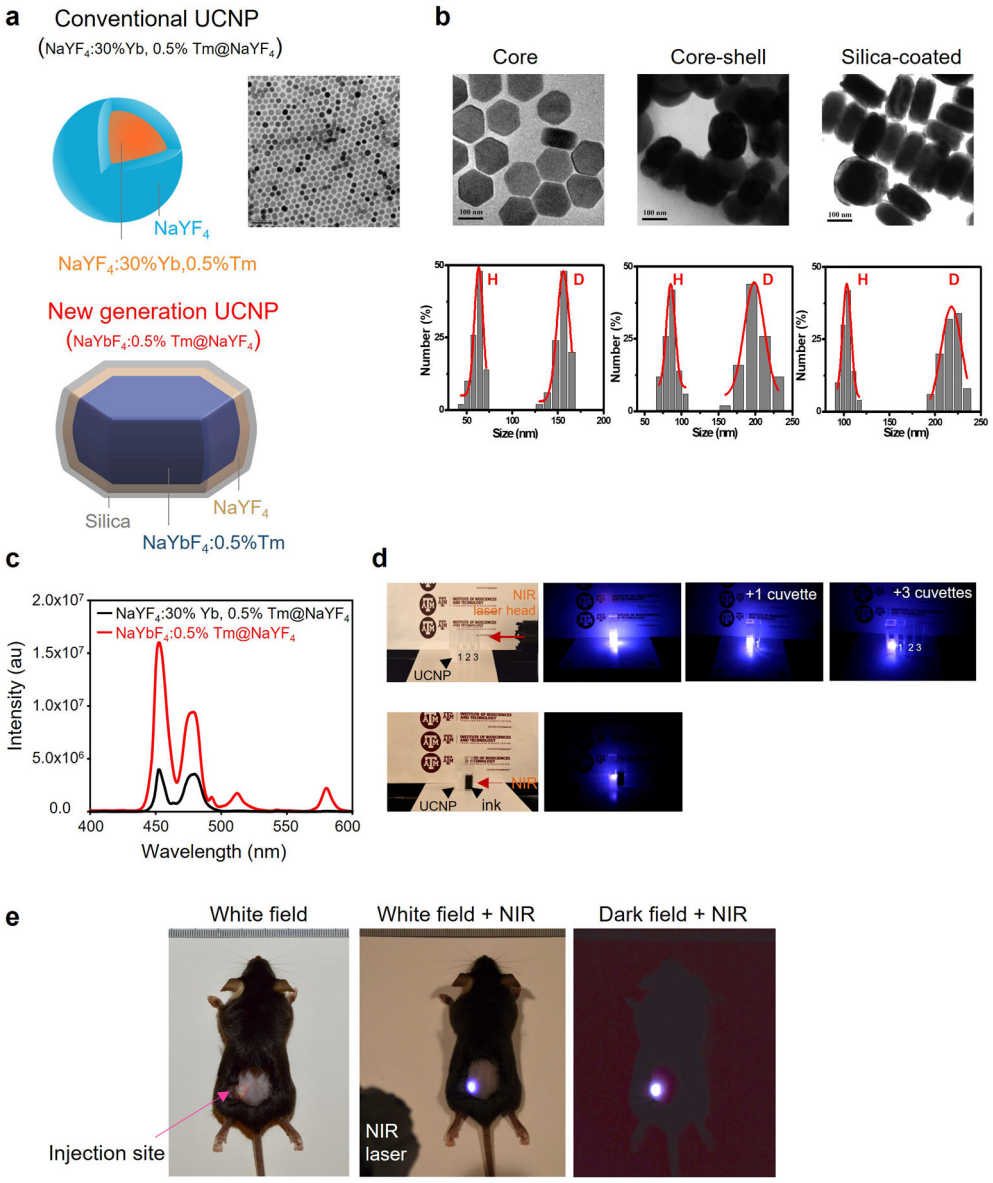

Extended Data Fig. 4. Optimization and characterization of synthesized UCNPs

a, Comparison of the the core/shell structures of synthesized UCNPs (*top*, β-$NaYF_4$:30% Yb, 0.5% Tm@$NaYF_4$; *bottom*, β-$NaYbF_4$:0.5%Tm@NaYF4) and TEM images (right). Scale bar, 100 nm.

b, TEM images and the size distribution (height denoted as "H" and diameter denoted as "D") of the $NaYbF_4$:0.5%Tm core nanoparticles (left), $NaYbF_4$:0.5%Tm@$NaYF_4$ core-shell nanoplates (middle), and silica-coated $NaYbF_4$:0.5%Tm@$NaYF_4$ core-shell nanoplates (right).

c, Comparison of the upconversion luminescence spectra of synthesized UCNPs upon NIR light illumination at 980 nm (*black*, β-NaYF4:30%Yb,0.5%Tm@NaYF4; *red*, β-

$NaYbF_4$:0.5%Tm@NaYF4 nanoplates). Their luminescence intensities were compared at the same condition with the same amounts of total lanthanide ions.

d, Blue light emitting from the leftmost cuvette containing UCNPs (β-$NaYbF_4$:0.5%Tm@NaYF4) upon NIR illumination. The UCNP-containing cuvette (leftmost) was placed next to the indicated numbers of H_2O-containing plastic cuvettes (labeled as 1, 2 and 3; *top*) or a cuvette containing dark ink (bottom). The NIR light source (980 nm) was placed on the right. Pictures were taken in a dark room except for the leftmost images. The light intensity was strong enough to illuminate the background after penetrating through cuvettes.

e, UCNPs emitted bright blue light locally at the injection site *in vivo* upon NIR light stimulation (980 nm; 250 mW/cm^2). Pictures were taken for the same mouse in the bright field without (left) or with NIR light (middle), or in the dark field with NIR light (right).

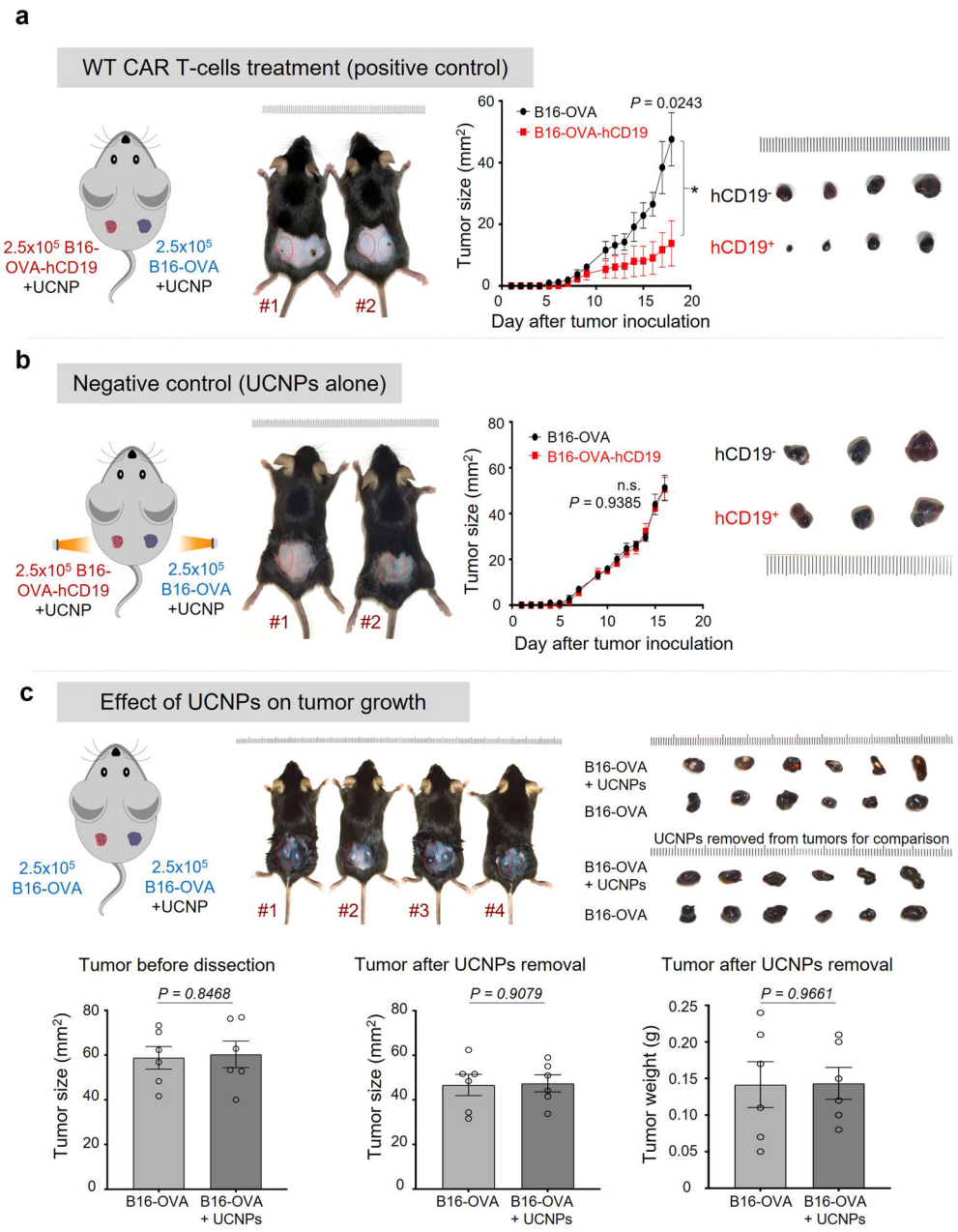

Extended Data Fig. 5. Effects of WT CAR T-cells and UCNPs on tumor growth

a, WT CAR-expressing $CD8^+$ T-cells selectively destroy CD19-positive melanoma tumors without light stimulation. *Left*, C57BL/6J mice were intradermally inoculated with $2.5x10^5$ B16-OVA-hCD19 cells in the left flank (red circle) and $2.5x10^5$ B16-OVA cells (CD19-negative tumor as control; blue circle) in the right flank. Two representative mice are shown after treatment with WT CAR T-cells + UCNPs for 8 days. *Middle,* Tumor sizes at the indicated time points were measured by a digital caliper with the tumor areas calculated in mm^2 (length x width). n = 4 biologically independent mice (mean ± s.e.m.). *P* values were calculated using two-sided unpaired Student's *t*-tests. *Right,* isolated B16-OVA and B16-OVA-hCD19 tumors at day 18.

b, The growth curves of B16-OVA-CD19/UCNPs and B16-OVA/UCNPs upon NIR light irradiation. *Left*, C57BL/6J mice were intradermally inoculated with $2.5x10^5$ B16-OVA-hCD19 cells in the left flank (red circle) and $2.5x10^5$ B16-OVA cells (CD19-negative tumor as control; blue circle) in the right flank. Two representative mice are shown after injection of UCNPs for 8 days without CAR T-cells under NIR treatment. *Middle,* Tumor sizes at the indicated time points were measured by a digital caliper with the tumor areas calculated in mm^2 (length x width). No significant difference in tumor size were observed. $P = 0.93$ when compared to the B16-OVA group at day 16 (unpaired two-sided Student's *t*-test; n = 3 biologically independent mice; mean ± s.e.m.). *Right,* isolated B16-OVA and B16-OVA-hCD19 tumors at day 16.

c, UCNPs did not affect tumor growth. C57BL/6J mice were intradermally inoculated with $2.5x10^5$ B16-OVA cells to each flank. Four representative mice were shown after injection with UCNPs to the right flank tumor. *Top right,* isolated B16-OVA and B16-OVA-UCNPs tumors before and after UCNP removals at day 18. *Bottom left and middle,* tumor sizes before tumor surgery (measured from outside the skin) and after UCNP removal, respectively, at day 18 were measured by a digital caliper with the tumor areas calculated in mm^2

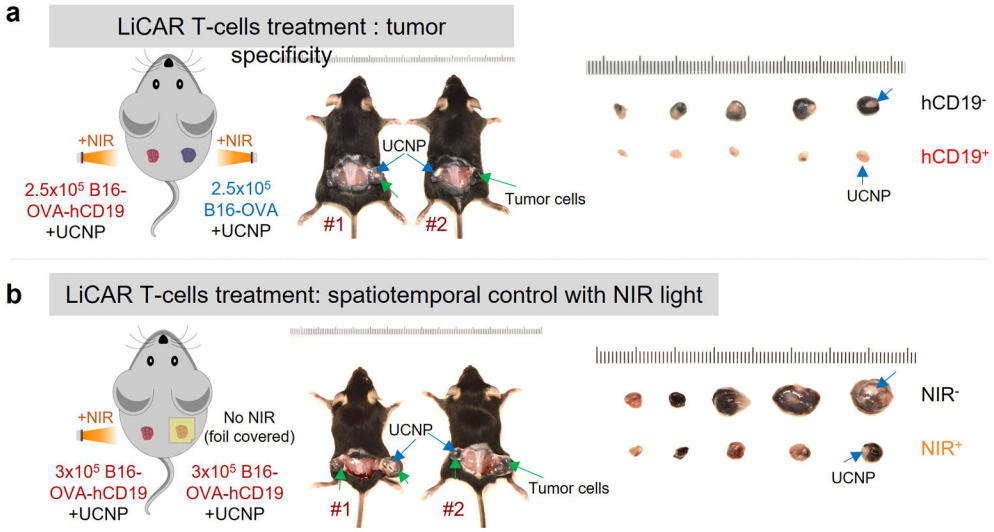

Extended Data Fig. 6. Light-inducible selective killing of $CD19^+$ solid tumors *in vivo* using LiCAR-expressing T cells

a, $CD8^+$ LiCAR T-cells selectively destroy CD19-expressing melanoma in response to NIR light illumination. *Left*, C57BL/6J mice were intradermally inoculated with $2.5x10^5$ B16-OVA-hCD19 cells in the left flank and $2.5x10^5$ B16-OVA cells (CD19-negative tumor as control) in the right flank. Two representative mice with opened tumor areas are shown after treatment with LiCAR T-cells + UCNPs and exposure to NIR pulses for 9 days. *Right,* isolated B16-OVA/UCNPs and B16-OVA-hCD19/UCNPs tumors at day 19. *Green arrow*, tumor cells. *Blue arrow*, UCNPs injected to tumor sites. The tumor masses after UCNP removal were shown in Fig. 3g.

b, LiCAR T-cells permit NIR light-inducible killing of B16-OVA-hCD19 melanoma in selected regions. *Left,* C57BL/6J mice were intradermally inoculated at both flanks with

3x10^5 B16-OVA-hCD19 cells. After injection with the LiCAR T-cells + UCNP mixture, the left flank was exposed to NIR pulses for 8 days, while the right side was protected from NIR light using aluminum foil. Two representative mice with opened tumors are shown at day 18. *Right,* isolated B16-OVA-hCD19/UCNPs tumors with and without NIR at day 18. *Green arrow*, tumor cells. *Blue arrow*, UCNPs injected to tumor sites. The tumor masses after UCNP removal were shown in Fig. 3h.

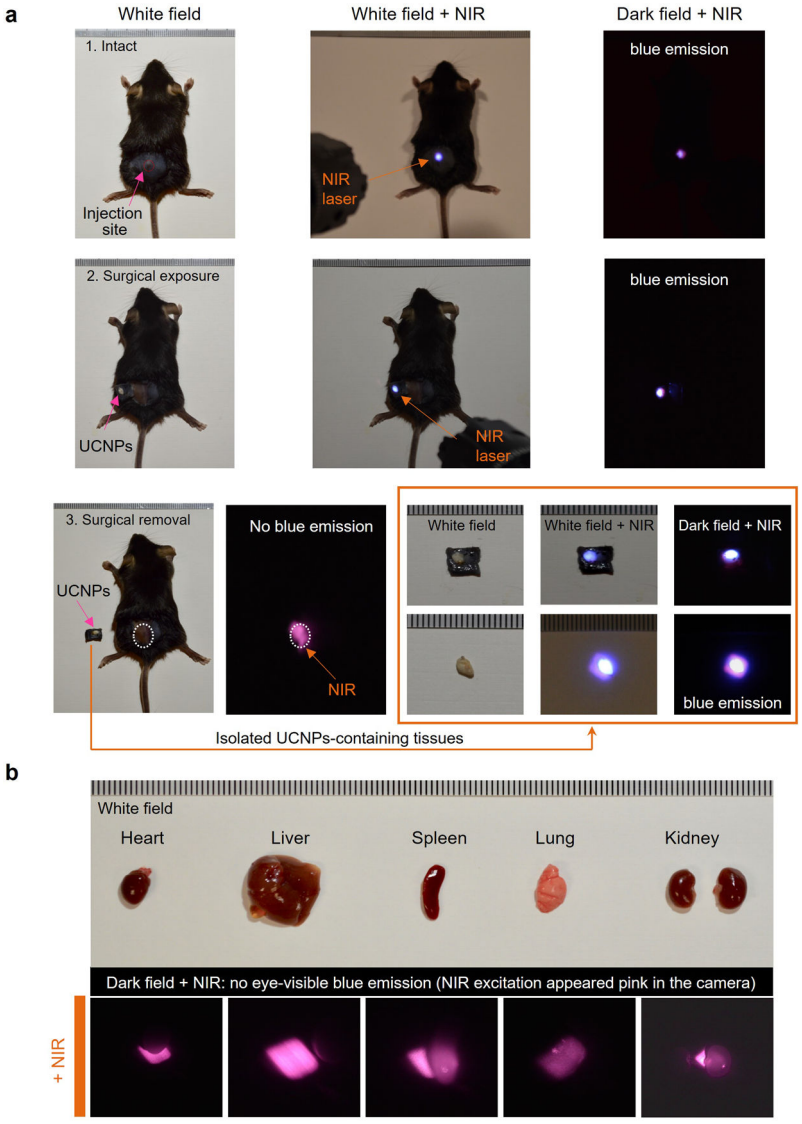

Extended Data Fig. 7. UCNPs are well confined within the injection site

a, Visualizing UCNPs after *s.c.* injection into the tumor sites under the indicated conditions. Images were acquired in the same mouse under three conditions: bright field without NIR light (left), bright field with NIR light illumination (middle) at the injection site (red arrow), or in the dark room with NIR light (right). *Top*, in situ images; *middle*, the UCNP-containing skin tissues were surgically exposed; *bottom*, after surgical removal. The NIR excitation showed a pink color in the camera if blue emission was not detected. Zoomed-in view on

the right (orange box): The UCNP-containing skin/tumor tissues (top) and well-confined UCNPs isolated from the tissue (bottom).

b, UCNPs did not spread to other major organs within the experimental window. Major organs were isolated from the mouse shown in panel **a** and then subjected to NIR light illumination. Only pink color was noted without blue emission, suggesting the absence of UCNPs in these tissues.

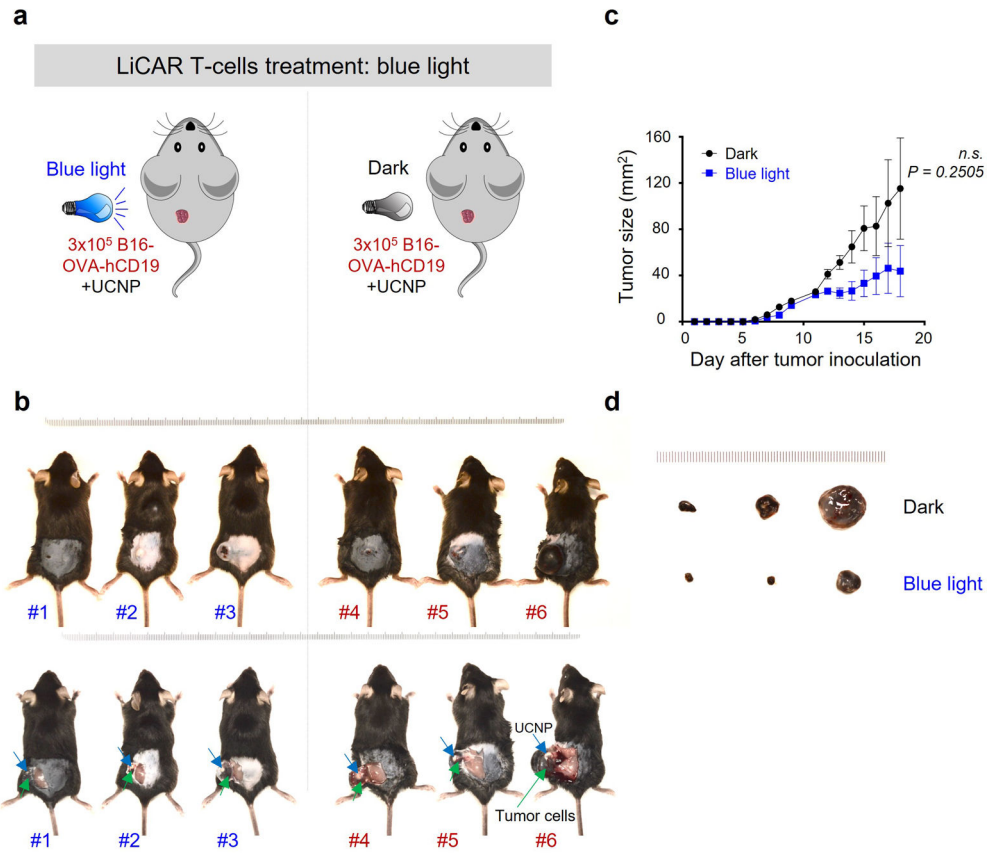

Extended Data Fig. 8. Blue light did not induce statistically significant changes in tumor killing

a, Cartoon illustrating the experimental setup. C57BL/6J mice were intradermally inoculated in the left flank with $3x10^5$ B16-OVA-hCD19 cells. After injection with the LiCAR T-cells + UCNP mixture, mice were either exposed to blue light (470 nm; 40 mW/cm^2, 2 hours per day) for 8 days, or kept in the dark.

b, Three representative mice from each group. The lower panel showed mice with opened tumors at day 18. *Green arrow*, tumor injection sites. *Blue arrow*, UCNPs in the tumor sites.

c, Measurements of tumor sizes at the indicated time points by a digital caliper. Tumor areas were calculated in mm^2 (length x width). n = 4 (dark group), n = 3 (light group) biologically independent mice (mean ± s.e.m.). *P* values were calculated using two-sided unpaired Student's *t*-tests. $P = 0.25$ when compared to the dark group at day 18.

d, Representative images of isolated B16-OVA-hCD19 tumors (shown in panel b) with and without blue light at day 18.

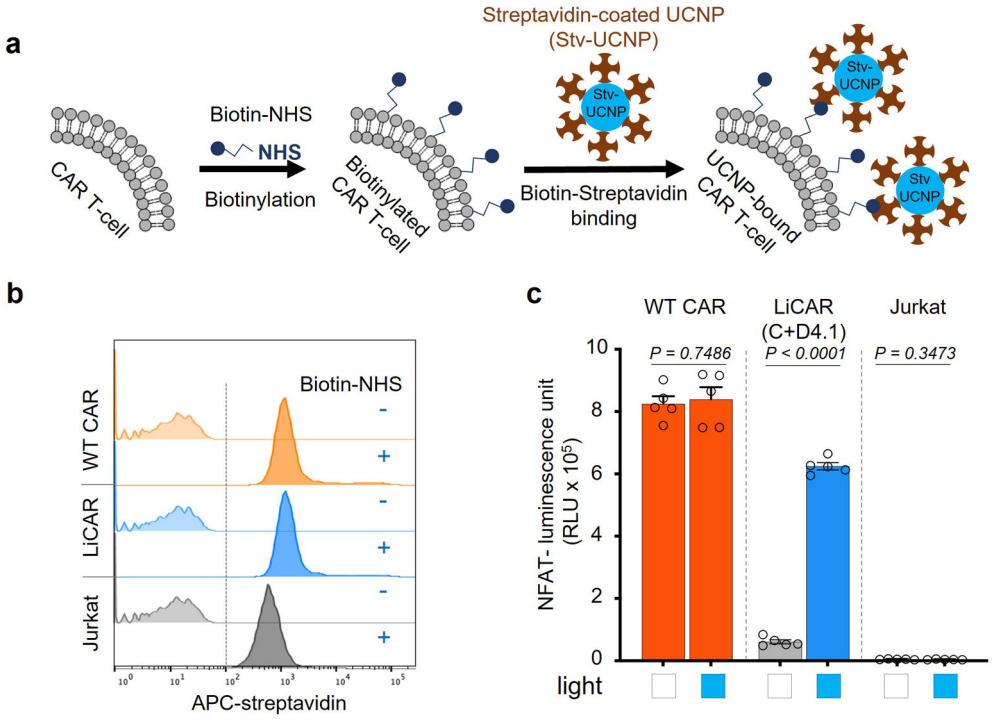

Extended Data Fig. 9. Biotinylated LiCAR T-cells remain fully functional and can be coupled with UCNPs that are surface coated with streptavidin (Stv-UCNPs)

a, Schematic illustration of surface biotinylation of engineered CAR T-cells and coupling with our previously-described UCNPs coated with streptavidin (Stv).

b, Flow cytometry analysis of biotinylation efficiency of Jurkat T cells expressing WT CAR and LiCAR. Engineered T cells were biotinylated with a high efficiency of over 98%.

c, Biotinylation did not affect engineered CAR T-cell activation. Quantification of NFAT-dependent luciferase (NFAT-Luc) reporter activity in engineered Jurkat T cells. LiCAR-transduced T cells engaged tumor cells bearing cognate antigen ($hCD19^+$ Raji cells) under dark (open box) or lit conditions (blue box). Blue light (40 mW/cm^2 at 470 nm) was applied for 20 min and then in pulsed cycles of 30 sec ON + 100 sec OFF for 8 h. n = 5 independent biological replicates (mean ± s.e.m.). *P* values were calculated using two-sided unpaired Student's *t*-tests.

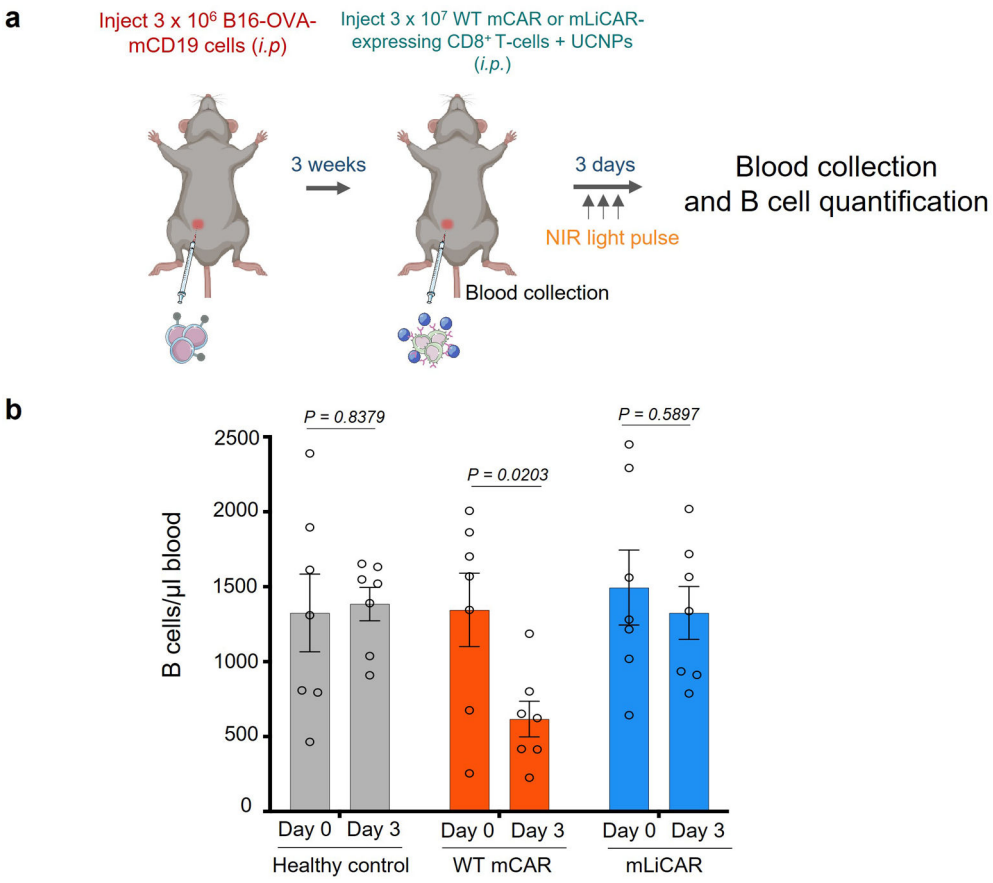

Extended Data Fig. 10. Intraperitoneal injection of mLiCAR T-cells to reduce "on-target off-tumor" side effects in a syngeneic mouse model of melanoma

a, Schematic illustration of the mouse model used to evaluate "on-target off-tumor" effects by intraperitoneal (*i.p.*) injection of B16-OVA-mCD19 tumor cells ($3x10^6$). After tumor growth for 3 weeks, WT CAR T cells/UCNPs or LiCAR-T/UCNPs cells that could engage mCD19-B16-OVA cells were subsequently injected into the tumor sites. LiCAR (combination of C + D4.1) T-cells treated mice were subjected to pulsed NIR light stimulation for 3 days (980 nm at a power density of 250 mW/cm^2; pulses of 20 sec ON, 5 minutes OFF; 2 h/day). On day 0 and day 3, blood was collected from the retro-orbital sinus by glass capillary from anesthetized mice for B cell quantification.

b, On-target off-tumor effects of mWT CAR and mLiCAR T-cells evaluated by the degree of B cell aplasia. Peripheral blood B cells from the WT mCAR or mLiCAR T-cell treated groups were counted and compared on day 0 and day 3. B cells from peripheral blood of healthy mice were used as control. n = 7 biologically independent mice (mean ± s.e.m.). *P* values were calculated using two-sided unpaired Student's *t*-tests.

Supplementary Material

Refer to Web version on PubMed Central for supplementary material.

ACKNOWLEDGEMENTS

We acknowledge Lara Strittmatter and the Electron Microscopy Facility at University of Massachusetts Medical School for EDS sample handling and analysis. We thank Stefan Siwko for manuscript editing. This work was supported by grants from the National Institutes of Health (R01CA232017 to Y.Z. and G.H., R01GM112003 to Y.Z., R01HL146852 to Y.H., R21GM138824 to Y.H., R01CA240258 to Y.H., R01AI040127 to A.R., and R01AI109842 to A.R.), the Department of Defense (W81XWH-19-1-0379 to G.H. and Y.Z.), the Cancer Prevention and Research Institute of Texas (RR140053 with Y.H. as a CPRIT Scholar in Cancer Research), the Welch Foundation (BE-1913-20190330 to Y.Z.), and the American Cancer Society (RSG-16-215-01-TBE to Y.Z. and RSG-18-043-01-LIB to Y.H.).

Data availability.

Supplementary Data are available online. The plasmids and reagents are available from the corresponding authors upon request. Source data are provided with the paper.

References

1. June CH, O'Connor RS, Kawalekar OU, Ghassemi S & Milone MC CAR T cell immunotherapy for human cancer. Science 359, 1361–1365, doi:10.1126/science.aar6711 (2018). [PubMed: 29567707]
2. Chmielewski M, Hombach AA & Abken H Antigen-Specific T-Cell Activation Independently of the MHC: Chimeric Antigen Receptor-Redirected T Cells. Front Immunol 4, 371, doi:10.3389/fimmu.2013.00371 (2013). [PubMed: 24273543]
3. Grupp SA et al. Chimeric antigen receptor-modified T cells for acute lymphoid leukemia. N Engl J Med 368, 1509–1518, doi:10.1056/NEJMoa1215134 (2013). [PubMed: 23527958]
4. Maude SL et al. Tisagenlecleucel in Children and Young Adults with B-Cell Lymphoblastic Leukemia. N Engl J Med 378, 439–448, doi:10.1056/NEJMoa1709866 (2018). [PubMed: 29385370]
5. Sadelain M, Brentjens R & Riviere I The basic principles of chimeric antigen receptor design. Cancer Discov 3, 388–398, doi:10.1158/2159-8290.CD-12-0548 (2013). [PubMed: 23550147]
6. Kochenderfer JN et al. B-cell depletion and remissions of malignancy along with cytokine-associated toxicity in a clinical trial of anti-CD19 chimeric-antigen-receptor-transduced T cells. Blood 119, 2709–2720, doi:10.1182/blood-2011-10-384388 (2012). [PubMed: 22160384]
7. Neelapu SS et al. Axicabtagene Ciloleucel CAR T-Cell Therapy in Refractory Large B-Cell Lymphoma. N Engl J Med 377, 2531–2544, doi:10.1056/NEJMoa1707447 (2017). [PubMed: 29226797]
8. Kennedy MJ et al. Rapid blue-light-mediated induction of protein interactions in living cells. Nat Methods 7, 973–975, doi:10.1038/nmeth.1524 (2010). [PubMed: 21037589]
9. Guntas G et al. Engineering an improved light-induced dimer (iLID) for controlling the localization and activity of signaling proteins. Proc Natl Acad Sci U S A 112, 112–117, doi:10.1073/pnas.1417910112 (2015). [PubMed: 25535392]
10. He L et al. Near-infrared photoactivatable control of Ca(2+) signaling and optogenetic immunomodulation. Elife 4, doi:10.7554/eLife.10024 (2015).
11. Wu J et al. An activating immunoreceptor complex formed by NKG2D and DAP10. Science 285, 730–732 (1999). [PubMed: 10426994]
12. Wu CY, Roybal KT, Puchner EM, Onuffer J & Lim WA Remote control of therapeutic T cells through a small molecule-gated chimeric receptor. Science 350, aab4077, doi:10.1126/science.aab4077 (2015). [PubMed: 26405231]
13. Irving BA, Chan AC & Weiss A Functional characterization of a signal transducing motif present in the T cell antigen receptor zeta chain. J Exp Med 177, 1093–1103 (1993). [PubMed: 8459204]
14. Zimmerman SP et al. Tuning the Binding Affinities and Reversion Kinetics of a Light Inducible Dimer Allows Control of Transmembrane Protein Localization. Biochemistry 55, 5264–5271, doi:10.1021/acs.biochem.6b00529 (2016). [PubMed: 27529180]

15. Chen J et al. NR4A transcription factors limit CAR T cell function in solid tumours. Nature 567, 530–534, doi:10.1038/s41586-019-0985-x (2019). [PubMed: 30814732]
16. Maraskovsky E, Chen WF & Shortman K IL-2 and IFN-gamma are two necessary lymphokines in the development of cytolytic T cells. J Immunol 143, 1210–1214 (1989). [PubMed: 2501391]
17. Yu N et al. Near-Infrared-Light Activatable Nanoparticles for Deep-Tissue-Penetrating Wireless Optogenetics. Adv Healthc Mater 8, e1801132, doi:10.1002/adhm.201801132 (2019). [PubMed: 30633858]
18. Tan P, He L, Han G & Zhou Y Optogenetic Immunomodulation: Shedding Light on Antitumor Immunity. Trends Biotechnol 35, 215–226, doi:10.1016/j.tibtech.2016.09.002 (2017). [PubMed: 27692897]
19. Nguyen NT et al. CRAC channel-based optogenetics. Cell Calcium 75, 79–88, doi:10.1016/j.ceca.2018.08.007 (2018). [PubMed: 30199756]
20. Barolet D Light-emitting diodes (LEDs) in dermatology. Semin Cutan Med Surg 27, 227–238, doi:10.1016/j.sder.2008.08.003 (2008). [PubMed: 19150294]
21. Ma Y et al. Targeting of antigens to B lymphocytes via CD19 as a means for tumor vaccine development. J Immunol 190, 5588–5599, doi:10.4049/jimmunol.1203216 (2013). [PubMed: 23630363]
22. Dai H, Wang Y, Lu X & Han W Chimeric Antigen Receptors Modified T-Cells for Cancer Therapy. J Natl Cancer Inst 108, doi:10.1093/jnci/djv439 (2016).
23. Lee DW et al. T cells expressing CD19 chimeric antigen receptors for acute lymphoblastic leukaemia in children and young adults: a phase 1 dose-escalation trial. Lancet 385, 517–528, doi:10.1016/S0140-6736(14)61403-3 (2015). [PubMed: 25319501]
24. Maude SL et al. Chimeric antigen receptor T cells for sustained remissions in leukemia. N Engl J Med 371, 1507–1517, doi:10.1056/NEJMoa1407222 (2014). [PubMed: 25317870]
25. Giavridis T et al. CAR T cell-induced cytokine release syndrome is mediated by macrophages and abated by IL-1 blockade. Nat Med 24, 731–738, doi:10.1038/s41591-018-0041-7 (2018). [PubMed: 29808005]
26. Allen ME et al. An AND-Gated Drug and Photoactivatable Cre-loxP System for Spatiotemporal Control in Cell-Based Therapeutics. ACS Synth Biol 8, 2359–2371, doi:10.1021/acssynbio.9b00175 (2019). [PubMed: 31592660]
27. Huang Z et al. Engineering light-controllable CAR T cells for cancer immunotherapy. Sci Adv 6, eaay9209, doi:10.1126/sciadv.aay9209 (2020). [PubMed: 32128416]

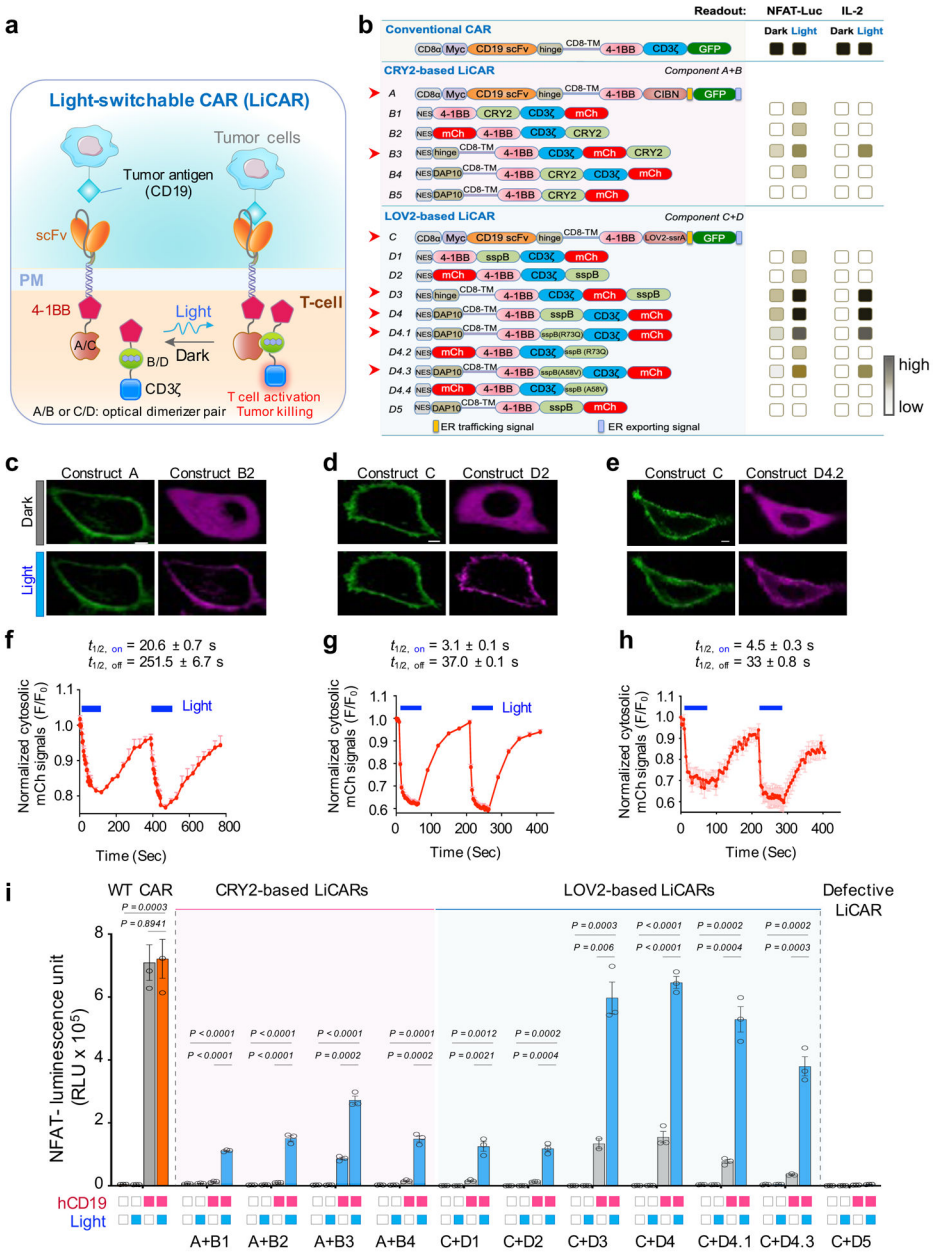

Figure 1 |. Design of light-inducible split CAR (LiCAR) T-cells.

a, Design of photoactivatable CARs that are dually gated by tumor antigen (CD19) and light. Engineered CAR T-cells can only be switched on in the presence of light when engaged with cognate tumor cells.

b, Optimized constructs used in the study (see Extended Data Fig. 1 for the full list). Modular domains within a typical CAR were split into two polypeptides (constructs A+B or C+D), the functional assembly of which can only be achieved upon light-induced interaction using two optical dimerizers (CRY2 + CIBN or LOV2-ssrA + sspB [or iLID]). Weaker versions of iLID (mutations R73Q or A58V in sspB; constructs D4.1-4.4) were used to reduce the degrees of LiCAR T-cell pre-activation. T cell activation was assessed using two independent assays: (i) NFAT-dependent luciferase (NFAT-Luc) reporter gene expression;

and (ii) IL-2 production upon incubation with cognate antigen-bearing tumor cells ($CD19^+$ Raji or Daudi lymphoma cells). The degree of activation was indicated by the darkness of the box on the right.

c-h, Representative confocal images (four images per each combination were taken), showing reversible recruitment of cytosolic Construct B or D (mCherry-tagged; magenta) toward the PM-resident Construct A (GFP-tagged; green; **c**) or Construct C (**d-e**) in response to two dark-light cycles (40 mW/cm^2; 470 nm) in Hela cells. (**f-h**) The activation and deactivation kinetics were indicated. n = 4 biologically independent cells (panel f); n = 36 biologically independent cells (panel g); n= 11 biologically independent cells (panel h; mean ± s.e.m.). Scale bar, 5 μm. Also see Supplementary Videos 1-2.

i, Quantification of NFAT-dependent luciferase (NFAT-Luc) reporter activity in Jurkat T cells expressing WT CAR, LiCAR, or defective LiCAR. Engineered T cells were co-cultured with tumor cells without (open box; human CD19-negative K562 cells) or with the CD19 antigen (red box; $hCD19^+$ Raji cells) under dark (open box) or lit conditions (blue box). Blue light (40 mW/cm^2 at 470 nm) was applied for 20 min and then in pulsed cycles of 30 sec ON + 100 sec OFF for 8 h. Defective LiCAR lacking the CD3ζ-ITAM domain was used as negative control. n = 3 independent biological replicates (mean ± s.e.m.). *P* values were calculated using two-sided unpaired Student's *t*-tests.

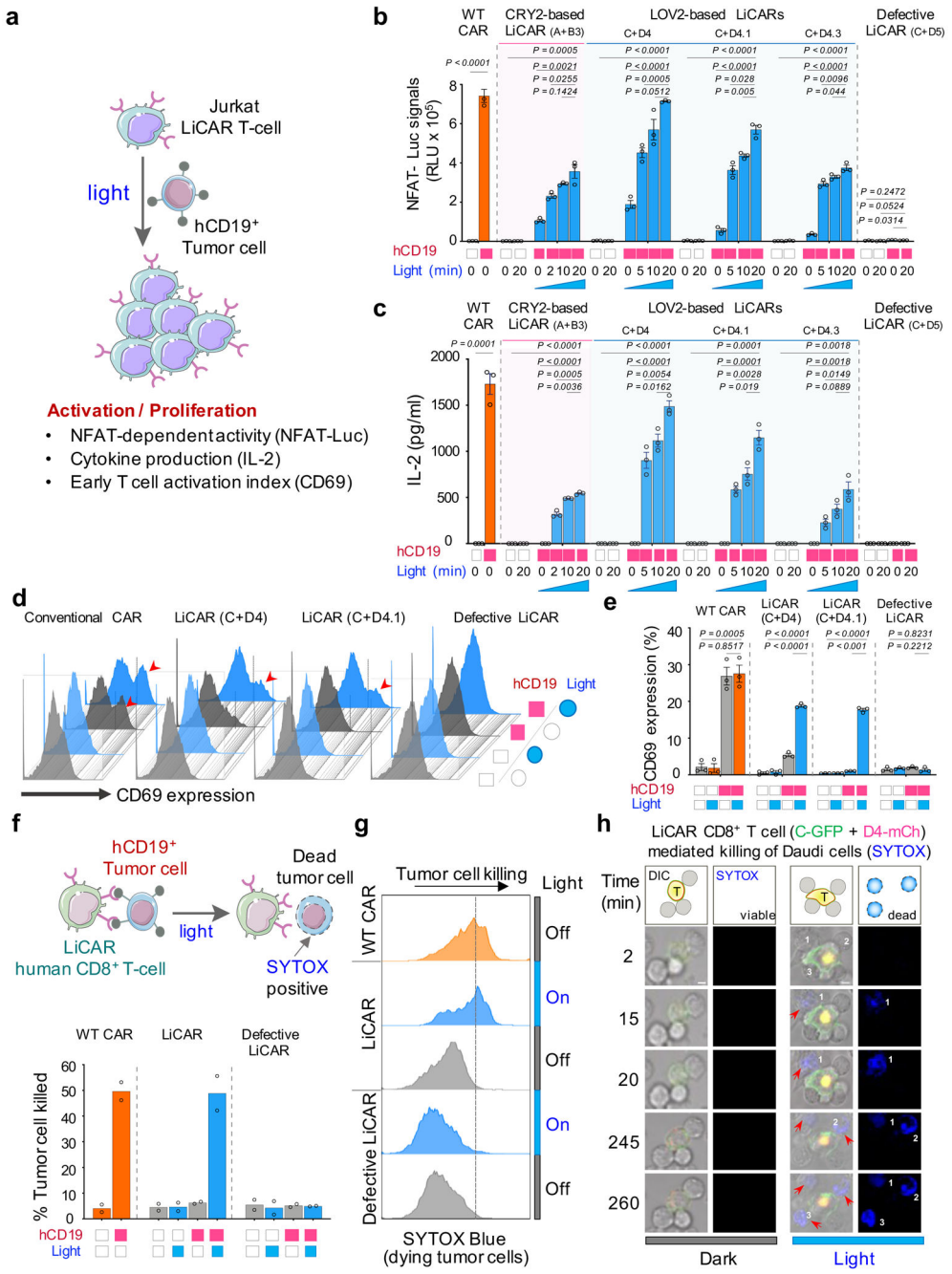

Figure 2 |. Photo-tunable immune response enabled by LiCAR T-cells.

a, Human Jurkat T cells were virally transduced to express WT CAR, LiCAR, or defective LiCAR, followed by functional assays to determine their therapeutic responses.

b-c, Light-tunable responses of engineered CAR T-cells examined by (**b**) photo-inducible NFAT-dependent luciferase reporter activity and (**c**) IL-2 production in Jurkat T cells. ON time of constant photostimulation was indicated. n = *3* independent biological replicates (mean ± s.e.m.). *P* values were calculated using two-sided unpaired Student's *t*-tests.

d-e, Determination of early T cell activation as reflected by upregulated CD69 expression on cell surface. Jurkat T cells transduced with conventional CAR, defective LiCAR, and LiCAR

were engaged with hCD19^{+} Daudi or hCD19^{-} K562 cells under dark or lit conditions. n = 3 independent biological replicates (mean ± s.e.m.). *P* values were calculated using two-sided unpaired Student's *t*-tests.

f, Primary human CD8^{+} T cells isolated from the peripheral blood of healthy donors were transduced to express WT CAR, LiCAR, or defective LiCAR, followed by functional assays (SYTOX Blue dead cell staining) to determine the tumor cell killing efficacy. The tumor killing results, quantified by SYTOX staining, were shown in the bar graph below the cartoon. n = 2 independent biological replicates.

g-h, Light-induced tumor cell killing assessed by flow cytometry (g) and time-lapse confocal imaging (h). Transduced human CD8^{+} T cells were engaged with hCD19^{-} K562 or hCD19^{+} Daudi lymphoma cells and kept in the dark or exposed to blue light. SYTOX blue was used to stain dying tumor cells with compromised plasma membranes. Shown in panel h are overlaid images of LiCAR-expressing human CD8^{+} T cells (green, C-GFP; red, D4-mCherry) engaged with Daudi cells (indicated by numbers; also see Supplementary Videos 3-6). Red arrowheads, dying Daudi cells with positive SYTOX blue staining. Cells were either kept in the dark or exposed to blue light (470 nm; 40 mW/cm^{2}; 5 h). Scale bar, 5 μm.

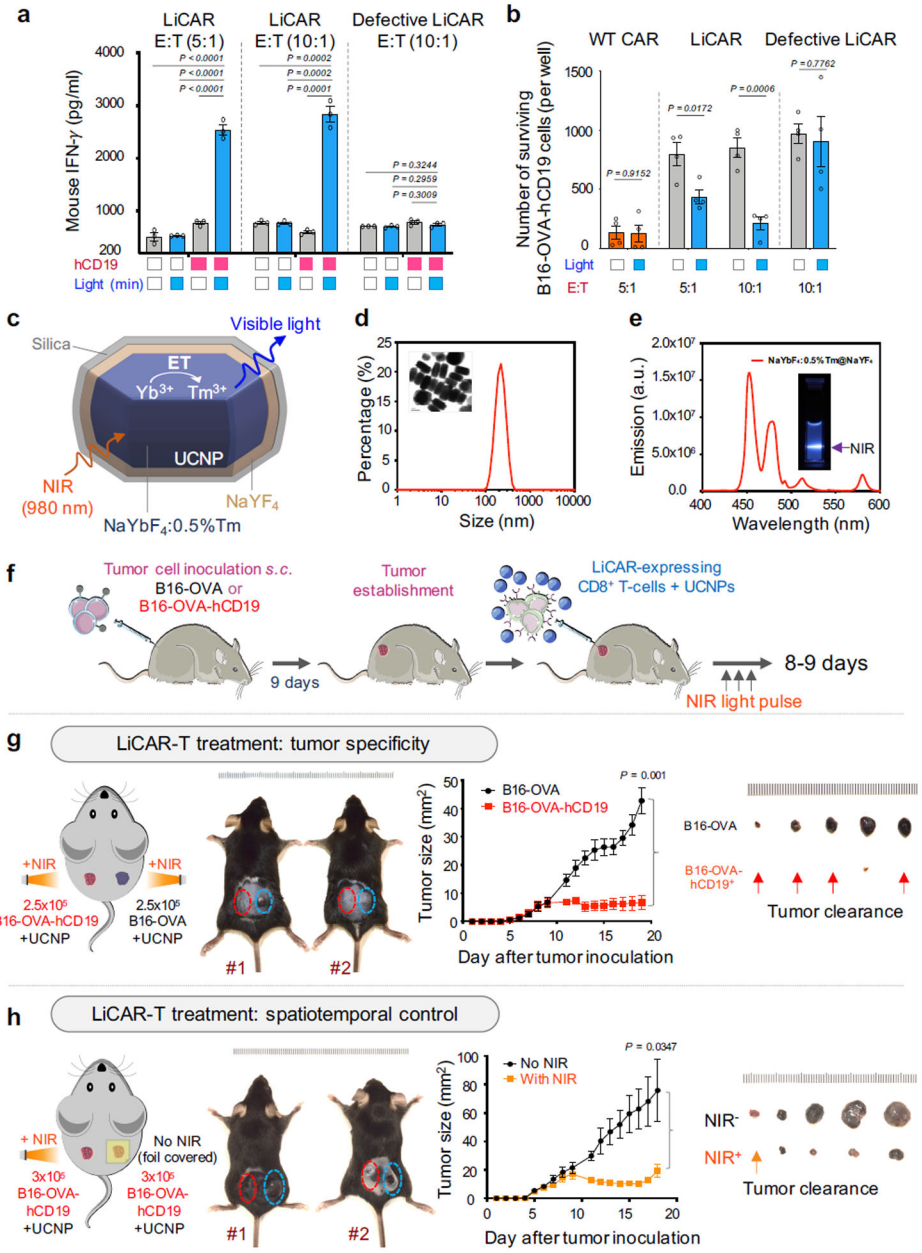

Figure 3 | A nano-optogenetic strategy for precise destruction of melanoma using LiCAR T-cells.

a, Quantification of IFN-γ produced by engineered mouse $CD8^+$ T cells expressing LiCAR or defective LiCAR after co-culturing with melanoma cells (B16-OVA cells expressing human CD19 [B16-OVA-hCD19] or B16-OVA [as control]) at different effector: target (E:T) ratios. n = 3 independent biological replicates (mean ± s.e.m.). *P* values were calculated using two-sided unpaired Student's *t*-tests.

b, B16-OVA-hCD19 cell killing efficacy of mouse $CD8^+$ T cells expressing WT CAR, LiCAR, or defective LiCAR at the indicated effector: target (E:T) ratios. n = 4 independent biological replicates (mean ± s.e.m.). *P* values were calculated using two-sided unpaired Student's *t*-tests.

c, Schematic of the core/shell structure of silica-coated upconversion nanoplates (UCNPs; $\beta NaYbF_4$: 0.5%Tm@$NaYF_4$).

d, Size measurement of silica coated β-NaYbF4:0.5%Tm@NaYF4 core-shell UCNPs by dynamic light scattering. The inset shows a representative transmission electron micrograph. Scale bar, 100 nm.

e, The upconversion luminescence spectrum of synthesized UCNPs upon NIR light stimulation at 980 nm.

f, Schematic of the *in vivo* experimental setup. $2x10^6$ mouse $CD8^+$ T cells expressing LiCAR and 150 μg of UCNPs were adoptively transferred into each tumor site of C57BL/6J mice 9 days after melanoma inoculation (B16-OVA or B16-OVA-hCD19). Mice were subjected to pulsed NIR light stimulation for 8-9 days (980 nm at a power density of 250 mW/cm^2; pulse of 20 sec ON, 5 minutes OFF; 2 h/day). At day 18 or 19, mice were euthanized for tumor isolation and phenotypic analyses.

g, LiCAR $CD8^+$ T-cells selectively destruct CD19-expressing melanoma in response to NIR light illumination. *Left*, C57BL/6J mice were intradermally inoculated with $2.5x10^5$ B16-OVA-hCD19 in the left flank (red circle) and $2.5x10^5$ B16-OVA cells (CD19-negative tumor as control; blue circle) in the right flank. Two representative mice are shown after treatment with $2x10^6$ LiCAR T-cells + 150 μg UCNPs and exposed to NIR pulses for 9 days. *Middle,* tumor sizes at the indicated time points were measured by a digital caliper with the tumor areas calculated in mm^2 (length x width). n = 5 biologically independent mice (mean ± s.e.m.). *P* values were calculated using two-sided unpaired Student's *t*-tests. *Right,* isolated B16-OVA and B16-OVA-hCD19 tumors at day 19. Also see Extended Data Figure 6a.

h, LiCAR T-cells permit NIR light-inducible killing of B16-OVA-hCD19 melanoma in selected regions. *Left,* C57BL/6J mice were intradermally inoculated at both flanks with $3x10^5$ B16-OVA-hCD19 cells. After injection with the $2x10^6$ LiCAR T-cells + 150 μg UCNP mixture, the left flank (red circle) was exposed to NIR pulses for 8 days, while the right side (blue circle) was protected from NIR light using aluminum foil. Two representative mice are shown at day 18. *Middle*, tumor sizes measured at the indicated time points. *Right,* isolated B16-OVA-hCD19 tumors with and without exposure to NIR light at day 18. n = 5 biologically independent mice (mean ± s.e.m.). *P* values were calculated using two-sided unpaired Student's *t*-tests. Note that more melanoma cells were injected so that we could collect sufficient tumor masses (without clearance as seen in panel h) for FACS analysis. Also see Extended Data Figure 6b.

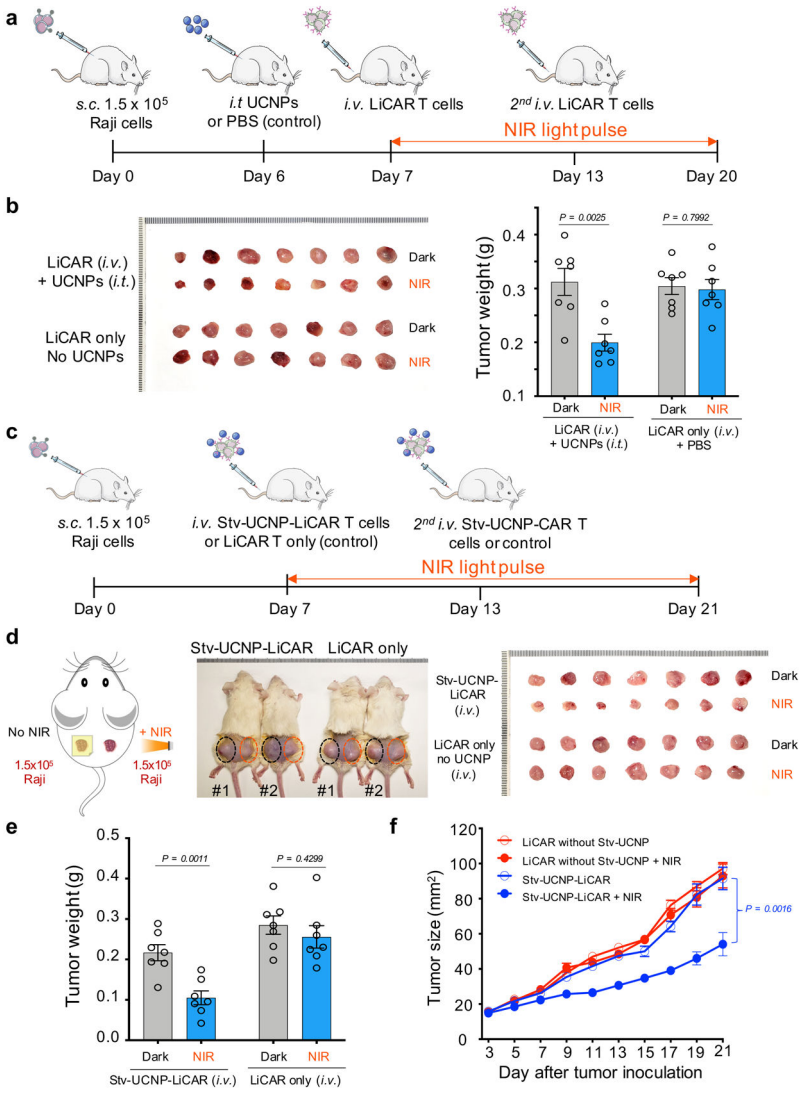

Figure 4 |. Systemic injection of LiCAR T-cells with UCNPs for NIR light-inducible lymphoma killing.

a, Schematic of the experimental setup for systemic injection of engineered CAR T-cells. $1.5x10^5$ Raji cells were subcutaneously (*s.c.*) inoculated to both flanks of SCID-Beige mice. After 6 days, 150 μg of UCNPs or PBS (control) were intratumorally (*i.t.*) injected into each tumor. Subsequently, 1 x 10^7 LiCAR-hCD8$^+$ T cells were systematically injected via tail vein injection (*i.v.*) at the indicated time points. Mice were subjected to pulsed NIR light stimulation for 13 days (980 nm at a power density of 250 mW/cm^2; 20 sec ON + 5 minutes OFF; 2 h/day). At day 20, mice were euthanized for tumor isolation and phenotypic analyses.

b, LiCAR T-cells (*i.v.*) coupled with UCNPs (*i.t.*) enable NIR light-inducible suppression of Raji lymphoma.

Left, representative images of isolated lymphoma tumors with and without exposure to NIR light from the mice treated with either LiCAR + UCNPs or LiCAR only at day 20.

Right, quantification of the tumor weight at the endpoint. n = 7 biologically independent mice (mean ± s.e.m.). *P* values were calculated using two-sided unpaired Student's *t*-tests.
c, Schematic of the experimental setup. $1.5x10^5$ Raji cells were inoculated to each flank of SCID-Beige mice. After 7 days, the mice were intravenously treated with $1 x 10^7$ streptavidin-UCNP-coupled LiCAR-$hCD8^+$ T-cells (Stv-UCNP-LiCAR) at the indicated time points. Mice were subjected to pulsed NIR light stimulation from day 7 to day 21 as mentioned above. On day 21, mice were euthanized for tumor isolation and phenotypic analyses.
d, Stv-UCNP-LiCAR T-cells selectively suppress Raji lymphoma with NIR light stimulation.
Left, SCID-beige mice were intradermally inoculated at both flanks with $1.5x10^5$ Raji cells in the form of Matrigel mixture, with the left flank shielded and the right flank exposed to pulsed NIR light illumination.
Middle, two representative mice from each group were shown at day 21.
Right, images of isolated lymphoma tumors with and without exposure to NIR light from xenograft mice treated with either UCNPs-conjugated LiCAR or LiCAR only at day 21.
e, Quantification of the tumor weight at the endpoint. n = 7 biologically independent mice (mean ± s.e.m.). *P* values were calculated using two-sided unpaired Student's *t*-tests.
f, Tumor growth curves for the indicated groups. Tumor sizes at the indicated time points were measured by a digital caliper with the tumor areas calculated in mm^2 (length x width). n = 7 biologically independent mice (mean ± s.e.m.). *P* values were calculated using two-sided unpaired Student's *t*-tests.

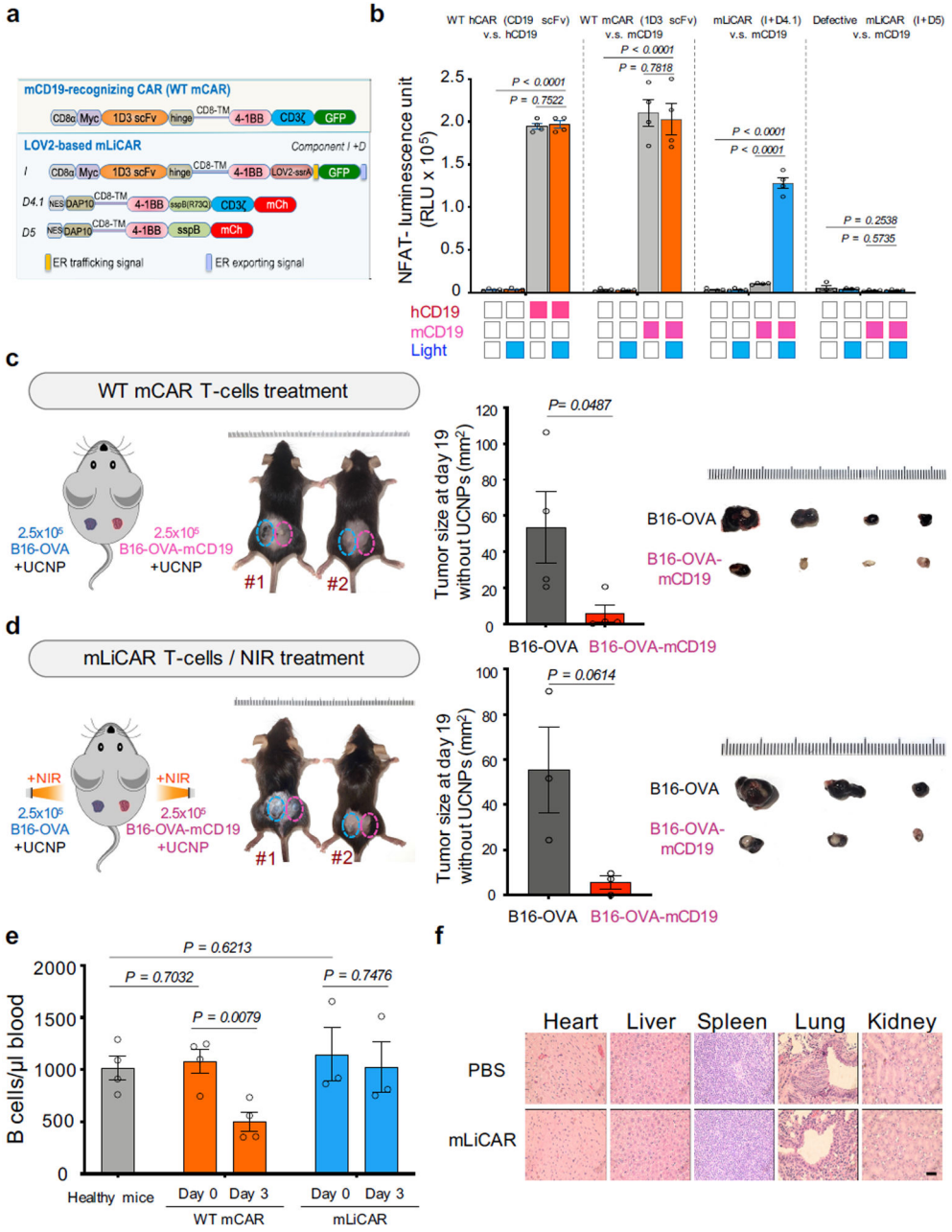

Figure 5 |. mLiCAR T-cells reduce "on-target off-tumor" effects in a syngeneic mouse model of melanoma.

a, Design of constructs to recognize mouse CD19 (mCD19) antigen overexpressed in B16 murine melanoma cells. The mCD19-recognizing scFv in WT mCAR or mLiCAR was derived a mouse mAb (clone 1D3).

b, The engagement of 1D3 scFv to mCD19 antigen was quantified by NFAT-dependent luciferase (NFAT-Luc) reporter activity in Jurkat T cells. Jurkat T cells transduced with human CD19 (hCD19)-recognizing (WT hCAR) or mouse mCD19 antigen-recognizing constructs (WT mCAR, mLiCAR, or defective mLiCAR) were engaged with the corresponding tumor cells bearing noncognate (open box; B16-OVA cells) or the cognate

antigens (B16-OVA-hCD19 for hCAR or B16-OVA-mCD19 for mCAR, mLiCAR, or defective mLiCAR groups) under dark (open box) or lit conditions (blue box). Blue light (40 mW/cm^2 at 470 nm) was applied for 20 min and then in pulsed cycles of 30 sec ON + 100 sec OFF for 8 h. n = 4 biologically independent mice (mean ± s.e.m.). *P* values were calculated using two-sided unpaired Student's *t*-tests.

c-d, WT mCAR- (**c**) or mLiCAR-expressing (**d**) murine CD8$^+$ T-cells selectively destroy mCD19-expressing melanoma cells *in vivo*. mLiCAR T-cells exhibit NIR-light dependent killing of B16-OVA-mCD19 tumor cells.

Left, C57BL/6J mice were intradermally inoculated with 2.5x10^5 B16-OVA cells in the left flank (as control without mCD19 overexpression, blue circle) and 2.5x10^5 B16-OVA-mCD19 cells (red circle) in the right flank. Mice were treated with WT mCAR T-cells + 150 μg UCNPs for 10 days (panel c), or 2x10^6 mLiCAR T-cells + 150 μg UCNPs with subsequent exposure to NIR pulses for 10 days (panel **d**).

Middle, Quantification of the tumor sizes. Tumor sizes at the endpoint after UCNP removal were measured by a digital caliper with the tumor areas calculated in mm^2 (length x width). n = 4 biologically independent mice for panel c and n = 3 biologically independent mice for panel **d** (mean ± s.e.m.). *P* values were calculated using two-sided unpaired Student's *t*-tests. *Right,* Representative images of isolated B16-OVA and B16-OVA-mCD19 tumors with UCNPs at day 19.

e, On-target off-tumor effects of mWT CAR and mLiCAR T-cells evaluated by the degree of B cell aplasia. Peripheral blood B cells from the WT mCAR or mLiCAR T-cell treated groups (as in panels **c-d**) inoculated with tumor cells were counted and compared on day 0 and day 3. B cells from peripheral blood of healthy mice were used as control. n = 4 biologically independent mice (mean ± s.e.m.). *P* values were calculated using two-sided unpaired Student's *t*-tests.

f, Representative H&E staining images of major organs isolated from mLiCAR T-cells/ UCNP/NIR treated mice bearing tumors or healthy mice subcutaneously administered with 100 μl PBS. The experiments were independently repeated four times. Scale bar, 100 μm.

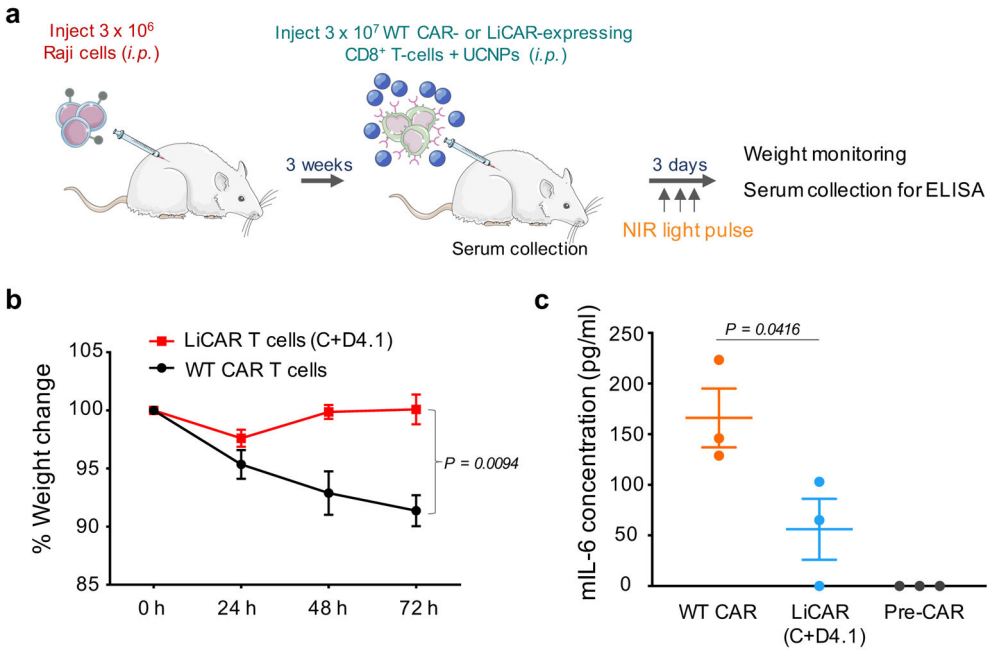

Figure 6 |. LiCAR T-cells mitigate cytokine release syndrome (CRS).

a, Schematic of the CRS experimental setup. Raji tumor cells ($3x10^6$) were injected (i.p.) into SCID-beige mice. After tumor growth for 3 weeks, WT CAR T cells/UCNPs or LiCAR T/UCNPs cells that could engage hCD19-expressing Raji cells were subsequently implanted to the tumor cell-injection sites. LiCAR (combination of C + D4.1)-treated mice were subjected to pulsed NIR light stimulation for 3 days (980 nm at a power density of 250 mW/cm^2 pulses of 20 sec ON, 5 minutes OFF; 2 h/day). Weight change was monitored daily. On day 0 (pre-CAR) and day 3, blood/serum was collected from the retro-orbital sinus by glass capillary from anesthetized mice.

b, Weight change of WT CAR T-cells/UCNPs or LiCAR T-cells/UCNPs/NIR-treated mice bearing Raji tumors. Weight of each mouse was normalized to the starting point before CAR T-cell implantation. n = 3 biologically independent mice (mean ± s.e.m.). *P* values were calculated using two-sided unpaired Student's *t*-tests.

c, ELISA measurements of the serum levels of mIL-6 at 72h after WT CAR T-cells/UCNPs or LiCAR T-cells/UCNPs/NIR treatment or before CAR T cell injection (Pre-CAR) into the SCID-beige mice. n = 3 independent biological replicates. (mean ± s.e.m.). *P* values were calculated using one-way ANOVA multiple comparisons.